SCHOOL OF ENGINEERING AND MATERIAL SCIENCE

CONJUGATE HEAT TRANSFER ANALYSIS OF A SMALL TURBOJET ENGINE COMBUSTION CHAMBER BY USING COMPUTATIONAL FLUID DYNAMICS

BY BIROL GUNDOGDU

150793966

AUGUST 26, 2016

SUPERVISOR: DR. LORENZO BOTTO
SECOND SUPERVISOR: Dr. TOM VERSTRAETE

SCOOL OF ENGINEERING AND MATERIAL SCIENCE

ENGINEERING/MATERIALS

AEROSPACE RESEARCH PROJECT

DENM003

DECLARATION

This report entitled “Conjugate Heat Transfer Analysis of a Small Turbojet Engine Combustion Chamber by Using Computational Fluid Dynamics” was written by me and all the simulations were done by me. Sources benefited from the others are fully reported in references. This report has not been submitted for any other qualification.

Name: Birol Gundogdu

Signed …….

Date: 26.08.2016

ACKNOWLEDGEMENTS

Firstly, I would like to express my Bachelor's degree supervisor Associate Professor Sitki Uslu, his assistant Ender Celik, and Associate Proffesor Mehmet Ali Guler because of their great support and encouragement, they really allocated their time and endeavoured on my group; Serhan Donmez, Mahmut Dogrudil, and Turkay Gencer.

Besides my old supervisor, I would like to thank Tusas Engine Industries (TEI) and its excellent engineers Ahmet Topal and Sinan Inanli on account of their great contributions.

I would like to thank my supervisor Dr. Lorenzo Botto and Dr. Tom Verstraete on account of directing me on the right way.

I would like to thank my Master's degree friends; Muhammed Said Hassan, Ayub Adan, Khalil Alassi, Sagar Chawla, Awais Ahmed Ijaz, Anees Tariq, Aamir Ishaque, Qaisar Khan, Ibn Mohammed, and Emran because of their sincerety and helping me a lot during my degree.

Additionally, I would love to thank my government because of supporting me during my degree with the scholarship provided me. During my degree, all my housemates from beginning to the end, I really thank them to be sympathetic and helpful, especially Husameddin Ates.

Finally, I would love to thank my family trusting me every time.

ABSTRACT

Turbojet engines have been in use since 1937. Each material used in this technology is very crucial and expensive. One of the most important component of turbojet engines is combustion chamber. Developments in this technology – high compression ratios- caused high temperature levels inside of combustion chamber and liner wall as well. To determine and to evaluate its temperature-dependent properties of the liner wall temperature is very crucial. In this work, a number of simulations have been done to see the parameters affecting liner wall temperature. The results were compared to experimental values obtained from tests. Firstly, the importance of gas properties as temperature-dependent was seen. Then, the fuel was used in gas and liquid phase, the liquid phase was decided to be used because evaporation energy and liquid flow affected flow and the magnitudes of temperature and velocity. Moreover, different combustion models by applying test case conditions were used and compared to experimental values. As a result, Presumed Probability Density Function combustion model was decided to be used in further works. Furthermore, different boundary layer conditions were used and compared to experimental values. As a result, the best compatible case with the test case was simulated in take-off conditions. The results obtained from this simulation was evaluated.

Key words: Conjugate Heat Transfer (CHT), Combustion Chamber, Multiphase Flow, Lagrangian Approach, Boundary Layer Thickness

Table of Contents

List of Tables

List of Figures

Abbreviations

1D : One-dimensional

2D : Two-dimensional

3D : Three-dimensional

AFR : Air-fuel Ratio

CC : Combustion Chamber

CFD : Computational Fluid Dynamics

DES : Detached Eddy Simulation

DNS : Direct Numerical Simulation

EBU : Eddy Break Up

JP-8 : Jet Petroleum

LES : Large Eddy Simulation

LHV : Lower Heating Value

LISA : Linearized Instability Sheet Analysis

NGV : Nozzle Guide Vane

OTDF : Overall Temperature Distribution Factor

PDF : Probability Density Function

PPDF : Presumed Probability Density Function

RANS : Reynolds Averaged Navier Stokes

RNG : Re-Normalisation Group

RTDF : Radial Temperature Distribution Factor

SMD : Sauter Mean Diameter

TAB : Taylor Analogy Break-up

U-RANS : Unsteady Reynolds Averaged Navier Stokes

Nomenclature

A : Area

C : Convection

C_p : Specific heat

CV : Control Volume

D : Diameter

D_a : Damköhler number

D_{an} : Diameter of Annulus

F : Fuel

g : Gravitational force

$h^0_{f,m}$: The heat of formation of the molecule 'm'

h_s : Enthalpy

H : Total entalpy

k : Turbulent kinetic energy

k_g : Thermal conductivity of gas

k_w : Thermal conductivity of liner wall material

K : Conduction

m_{air} : Air mass flow rate

m_{fuel} : Fuel mass flow rate

O : Oxidizer

p : Pressure

P : Products

P_k : Source term

r : Radius

R : Gas constant

Re : Reynolds number

S : Surface

Sc_{kt} : Turbulent Schmidt number

S_{ij} : Strain tensor

S_E : The heat transfer between gas and liquid form of the fluid

S_H : The heat generated by reactions

T : Temperature

t : Time variable

U : Velocity magnitude

$u^{'}$: Turbulence intensity

V : Volume

Y_k : Species mass fraction

Z : Mixture fraction

x, y, z : Cartesian coordinates

α : The thermal diffusivity

ε : Eddy dissipation rate

η_k : Kolmogorov scale

τ_k : Kolmogorov time scale

ν_k : Kolmogorov velocity scale

Φ : Any scalar

μ : Viscosity

μ_t : Turbulent viscosity

ν : Kinematic viscosity

Ω : Loading factor

$\omega_{r,n}$: The speed of reaction

$v^{''}_{m,n}$: The mole fraction of the molecule ‘m’ in the reaction n^{th}

$v'_{m,n}$: The mole fraction of the molecule ‘m’ in the reaction n^{th}

1. INTRODUCTION

From beginning of human life, people watched flying animals and wanted to mimick their actions in order to fly. Then, some people tried to fly by designing some fundamental air vehicles like balloon, zeppelin, and glider. Leonardo da Vinci designed some air vehicles without thinking scientific values in 1500s. After discovering hydrogen gas and some of its useful properties, it was used for hot-air balloon by Montgolfier brothers. After several suggested theories in mechanics, and fluid dynamics by scientists, those developments caused to the foundation of aerodynamics. In the 19th century, many engine technologies had been developed by engineers, and scientists. Gliders were tried to fly at that time. These developments made Wright Brothers think about powered flight. The modern aircraft design with tail and engine was succeeded by Wright Brothers in 1909. The engine used by Wright Brothers was a reciprocating engine. The need for more power required much bigger engines and that caused the invention of modern jet engine by two different scientists at the same time. Frank Whittle applied for a patent for the first turbojet engine in 1930, later on, Hans Joachim Pabst von Ohain designed and manufactured fir operational jet engine in 1937. [1] Then turboprop, turboshaft and turbofan engines were invented and used in different applications. In recent years, ramjet and scramjets are under development.

1.1. Modern Turbojet Engines

Frank Whittle submitted his patent application in 1930 and he manufactured its prototype and made its tests in 1937. [1] The results obtained from tests were successful and led to jet engine technology development. Almost the same time, Hans Joachim Pabst von Ohain designed and manufactured first aircraft with turbojet engine in 1939. [1] These two jet configurations made great contributions for aerospace engine technologies. Also it is stated that these inventions affected the Second World War in terms of politics. [2]

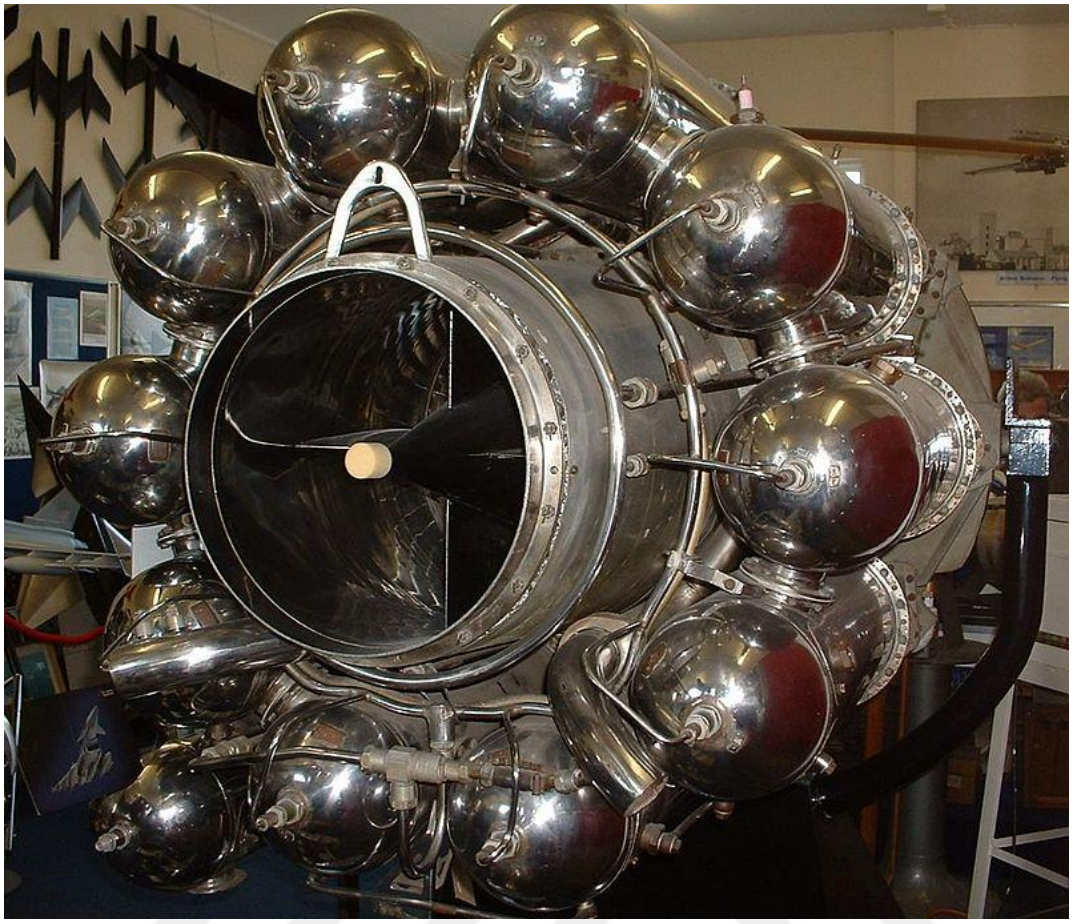

Figure 1: The first turbojet engine designed by Frank Whittle [3]

Figure 2: The first aircraft flying with turbojet engine by Von Ohain [4]

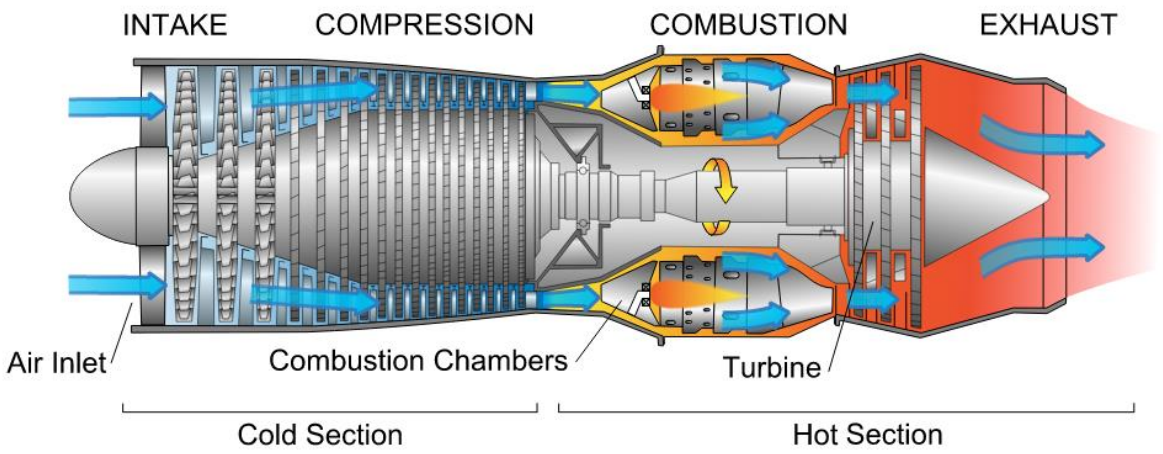

Figure 3: Diagram of a typical gas turbine jet engine [5]

As shown in the figure 3, a modern gas turbine jet engine consists of 5 main parts which are called as air intake (diffuser), compressor, combustion chamber (combustor), turbine, and exhaust (nozzle). Brayton cycle defines the cycle in terms of T-s diagram or P-v diagram.

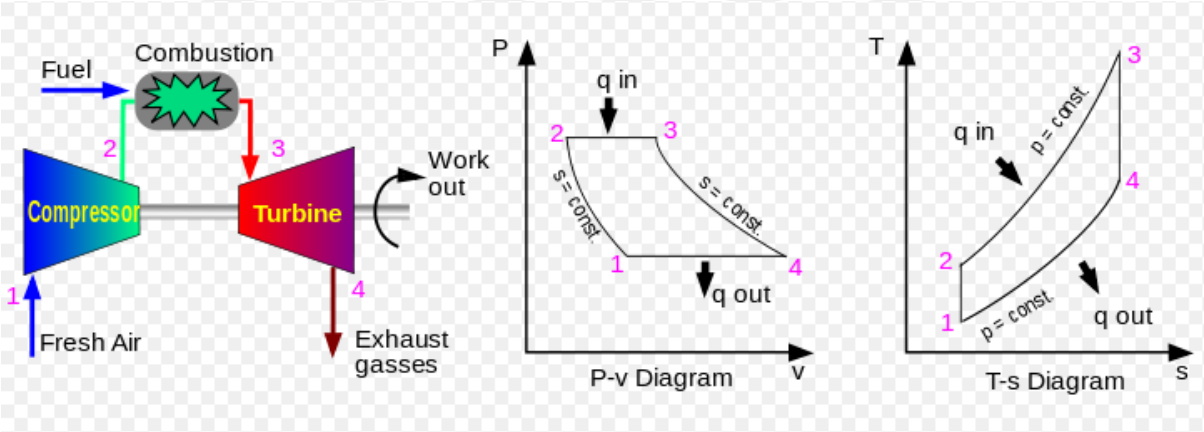

Figure 4: Diagram of Brayton cycle [6]

The idealised diagrams for Brayton cycle is shown in the figure 4. Brayton cycle is used to see performance parameters, but in reality, all components of jet turbine engine has different efficiencies, so the Brayton cycle could have errors.

The main aim of a turbojet engine is to obtain maximum thrust, by increasing all component's efficiencies. The principle of thrust is explained by 3rd Newton's law of motion. Basically, the difference between outlet velocity of hot

gas and inlet velocity of the air. When the thrust obtained from engines equals to drag force on the aircraft body, the velocity of the aircraft becomes constant due to 3rd Newton's law of motion. Also in order to reach equilibrium condition, the lift force has to equal to total weight of the aircraft.

The air coming from outside is taken to air intake (diffuser), in this part air expands, velocities of flow particles go down, then the air goes to compressor. In modern applications, both for turboprop, turbofan, turbojet engines, and axial compressors are used to compress the air. In small engines centrifugal compressors are widely used because of volume limitations. While the compression ratio of one stage of an axial compressor is around 1.15, the same ratio is around for a centrifugal compressor is around 4, but in practice, just 2 stage centrifugal compressors are in use. In the beginning of the engine performance analysis, one stage centrifugal compressor was used for the engine which will be analysed. After compression, the compressed air goes to combustion chamber, in this section, the fuel injected into the chamber is burned with this air. Then, the hot gas goes to turbine blades, and in this section, the air expands due to the structure of the turbine blades. The compressor and the turbine are joined each other with a shaft. In some applications, there are more than one compressor and one turbine. After expanding in the turbine, the hot gas goes to the exhaust (nozzle). The geometry of a nozzle is designed to reach Mach number (1) at the exit in order to get maximum thrust. [7]

1.2. Combustion Chamber Components

A combustion chamber consists of several components which are called; case (or casing), diffuser, liner, dome, swirler, fuel injector, igniter. Additionally, there are four air flows can be seen in a typical combustion chamber, they are called primary air, intermediate air, cooling air, and dilution air. Furthermore, the combustion chamber zones can be identified as hot flow and cold flow. These definitions will be explained after given their basic frames.

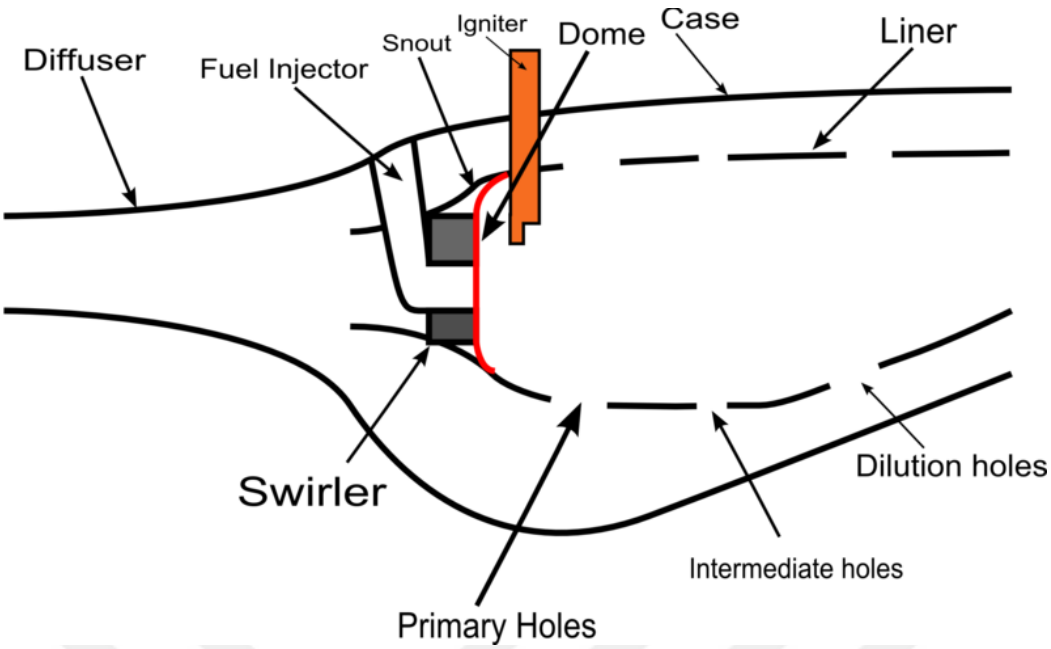

Figure 5: Combustion Chamber Components [8]

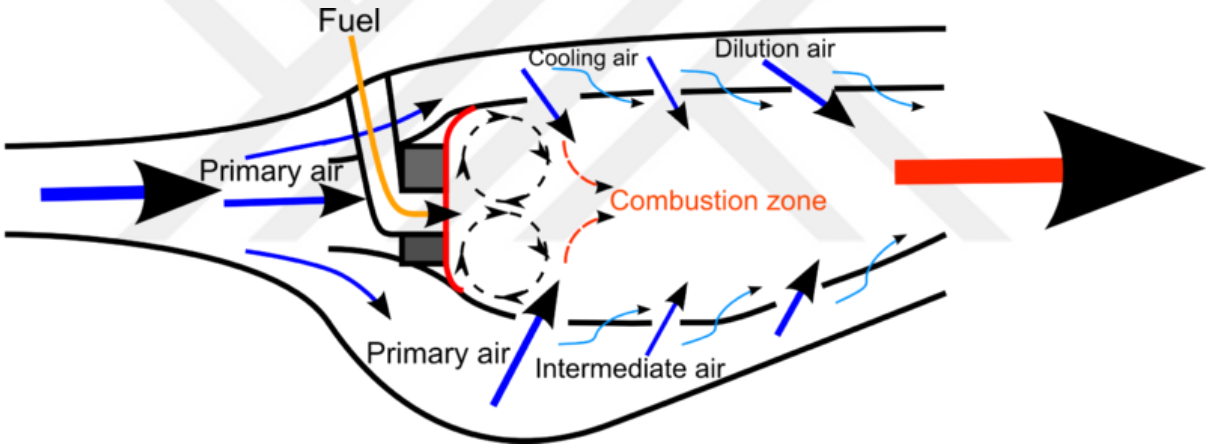

Figure 6: Combustion Chamber Zones [8]

The case or casing is the outer shell, which has a very simple geometry, protects the combustion zone from external forces and effects.

The compressed air coming from compressor has high speeds, in the diffuser part the velocity of cold air is decreased and is aimed to be suitable for combustion. The most common problems are boundary layer separation and unwanted vorticities.

Liner is the metal separating hot flow and cold flow. The most common problems related to liner is cooling and high thermal forces on it. In this thesis,

the liner wall temperature computing is aimed to found by using different combustion models and boundary layer properties.

Dome and swirler are located between primary air and primary zone which combustion starts and mostly completed in. The main purpose of swirler is to have good fuel-air mixing. Fuel injector is used to inject fuel. There are several types of injectors widely used in the industry. Some of them are pressure-atomizing, air blast, vaporizing, and pre-vaporizing injectors. Spray characteristics, liquid particle diameters are very important design criteria for injectors. Igniter is used to ignite the mixture.

Moreover, the combustion chamber hot flow can be separated three zones which are called as primary, secondary, and dilution zones. Combustion is desired to start in primary zone, to finish in secondary zone and to be cooled in dilution zone in order to be suitable for turbine blades.

1.3. Combustion Chamber Types

There are three types of combustion chambers mainly: Can-type combustor, cannular (or tubo-annular) combustor, annular combustor. The corresponding geometries are shown below.

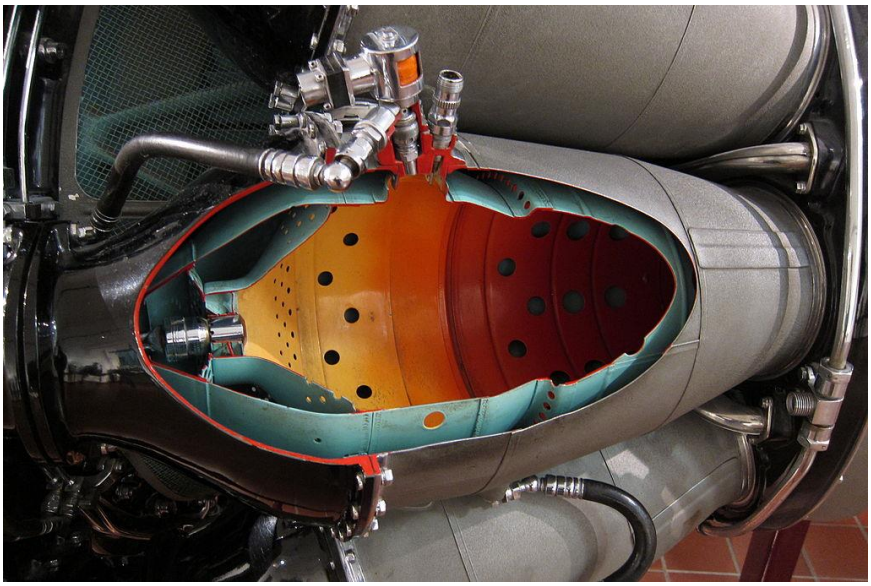

Figure 7: Can type combustor [9]

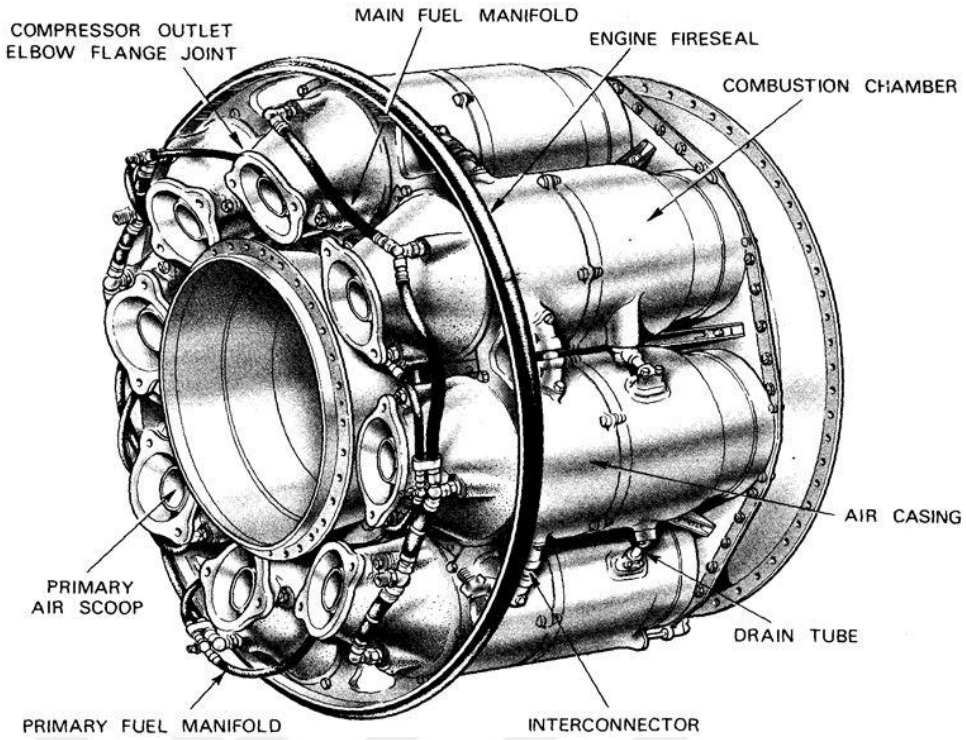

Figure 8: Cannular type combustor [10]

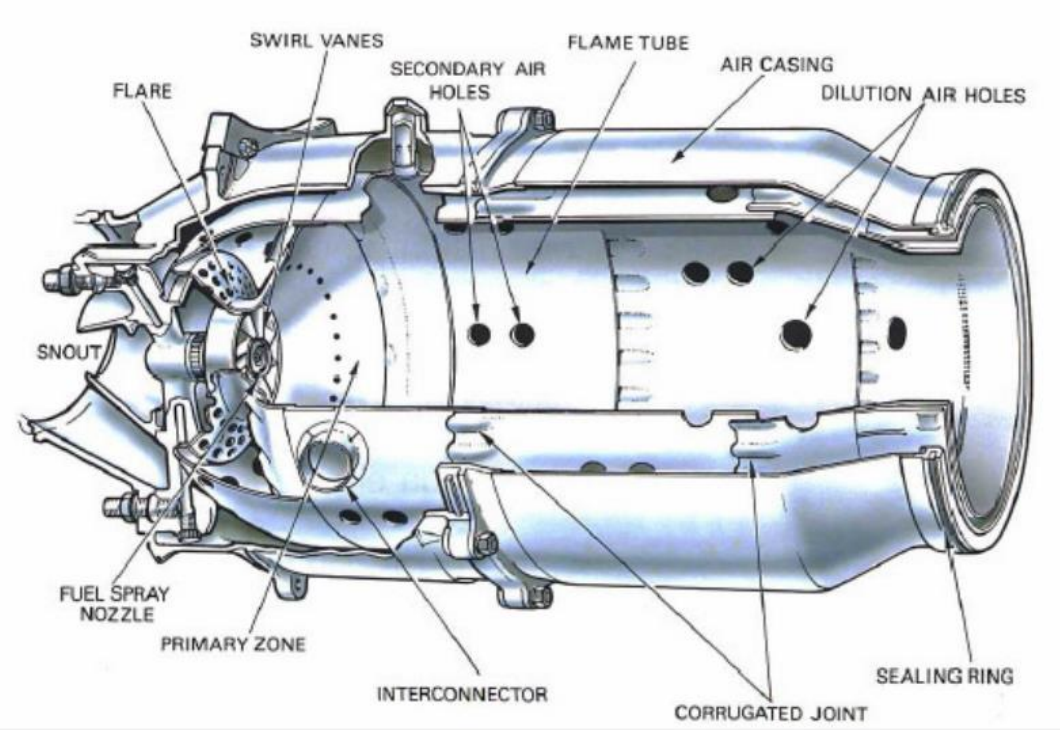

Figure 9: Annular type combustor [11]

1.4. Literature Survey

As mentioned before, there are three types of combustion chamber widely used in the industry. In order to perform needs, an annular combustion chamber geometry was created by the industry, Tusas Engine Industries, this geometry was created by considering many design criteria, and taking into account combustion chamber problems have been confronted up to now. Many simulations have been made up to now, as a result there is a huge information library in books, journals and conference notes. By using some of this information, the simulations will be done for the geometry.

Lawson [12] succeeded the first combustion chamber analysis by defining reactions by using Computational Fluid Dynamics. He also stated that to make CFD analysis reduces 1 month of manufacturing time and cost as 50000 U.S Dollars.

According to Lefebvre [13], there are many design criteria that should be satisfied by the geometry. These criteria can be put in order as following:

- High combustion efficiency
- Reliable and smooth ignition
- Wide stability limits
- Low pressure loss
- Outlet temperature distribution
- Low emissions (NOx, CO …)
- Freedom pressure pulsations and any instability
- Size and shape compatibility
- Minimum cost and ease of manufacture
- Maintainability
- Durability
- Multi-fuel capability

Additionally, HIH Saravanomutto et al. [7] added some criteria should be satisfied by the geometry, they are;

- Low outlet temperatures at exit, the temperature distribution should be suitable for turbine blades, and also this criteria can be calculated by two terms; OTDF, RTDF.
- Avoiding carbon deposits,
- Avoidance of smoke,
- Heat resisting systems,
- Long life-time; at least 10000 hours operating time for aircraft engines.

Walsh and Fletcher [15] also added some important criteria to design a new combustion chamber, here are the parameters should be satisfied;

- Reducing Mach Number at compressor exit and combustor inlet,
- Mach number should be around 0.3 around dilution air holes to have good penetration.
- Combustion and flame stabilisation,
- Combustion should start in the primary zone and finish in secondary zone.

Walsh and Fletcher [15] also stated that pressure loss between the inlet and outlet of the combustor should be between 2% and 4%, but in some applications it can be taken up to 5%.

There is an important design parameter called the loading factor, the heat capacity of a combustion chamber. Walsh and Fletcher [15] suggested that the loading factor should be less than 100 $kg/s.atm^{1.8}.m^3$.

Combustion intensity is a measure of the rate of heat release per unit volume, and it is suggested to be less than 60 MW/m^3.atm according to Walsh and Fletcher [15].

Residence time is the time spent by a fluid particle inside of combustion chamber and is suggested by Walsh and Fletcher [15] to be around 3 milliseconds in order to have efficient combustion. But the residence time depends on geometry, temperature, and velocities; so it could be around 3 milliseconds.

Among these design criteria, there might be some problems while performing some criteria. In this dissertation the geometry was designed by thinking all these criteria, and aimed to compute wall temperature by using different methods suggested or experienced in the literature.

According to HIH Saravanomutto et al. [7], the liner wall receives energy from the hot (burned) gases and flame by convection and radiation. The liner wall is cooled by cooling air coming from the cold section by the same way; convection and radiation. There are some ways to cool the liner wall, one method to achieve this aim is to leave narrow angular gaps between overlapping sections of the flame-tube. Another method to cool liner wall is to use small holes with an internal splash ring. A modern method is the use of transpiration cooling; this method allows cooling air to enter in flame tube.

Arthur H. Lefebvre [13] stated that liner wall must be strong enough for the buckling load created by pressure differences, and also thermal resistance due to continuous and cyclic high temperatures. This is achieved by using high temperature, anti-oxidant composite materials like Ni-Co-Fe based. Approximately 40 % of the air is used to cool the liner wall. He also stated that the liner wall temperature can be thought as constant after some time passed in operation. There are mainly 5 components of heat transfer; convection and

radiation from hot gases to liner; conduction inside of the wall; convection and radiation from liner to cold gases.

Arthur H. Lefebvre [13] stated that the importance of cooling liner wall is getting much more important than before because of high pressure ratios in compressors. High pressure ratio makes the inlet temperature of the combustion chamber so it is necessary to reduce liner wall temperature to some identical values. Higher inlet temperature causes high temperatures around the flame and primary zone. This is the main reason of high heat transfer by convection and radiation from hot burned gases to the liner wall. Furthermore, high inlet temperature makes the cooling air less efficient. Additionally, more air can affect the temperature distribution at exit, and this may cause problems in turbine blades because of high thermal forces around the tip and hub sides of blades.

Lefebvre and Norster [16] made some experimental studies on the pressure loss on liner and good mixing of air and fuel. They discovered that in order to have good fuel-air mixing, the liner cross-sectional area should have an experimental ratio when compared total cross-sectional area of the combustor. These correlations were cared while designing the geometry in conceptual design process.

Kaddah [17] made some experiments on discharge coefficients, and he suggested that the Mach number of the secondary air channel should be less than 0.1 Mach. He also made some correlations on different type of holes like rectangular shape. Freeman [18] modified Kaddah's correlations for plunged geometries.

Carotte and Stevens [19] examined air jet penetrations and velocities. They made some correlations on these configurations.

Sauter [20] made some experiments on spray analysis, and he suggested that fluid particles have different diameters and this affects whole combustion. His theory is called the Sauter Mean Diameter (SMD). SMD can be defined as the ratio of total volumes of spray particles to total surface area of all these particles.

Mouldi Chrigui et al. [21] discovered that ambient pressure affects the diameters of liquid particles and their velocities. They stated that if the pressure of combustor increases, the diameters of particles also increases, and this affects the combustion. Additionally, up to 5 bar of ambient pressure, the pressure does not affect remarkably droplet evaporation; however, after 5 bar of ambient pressure, the turbulence intensity grows unexpectedly. The numerical studies were compared to experiments, and they obtained a good agreement. Furthermore, according to experiments done under 5 bar of ambient pressure, the droplet diameters are around 20 micrometres, and the velocities of particles have 4 m/s axial velocity in the spray direction. If the ambient pressure is greater than 5 bar (the experiments done at 10, 15, and 18 bar), the axial velocity of droplets decreases so fast, the maximum velocities are around 2 m/s. In the analysis, average droplet diameters will be taken as 20 micrometres, and average velocity will be used 4 m/s in axial direction.

There are some different types of injectors in the industry, and one type of them is hollow cone injector. Ahmad Hussein Abdul Hamid et al. [22] made some experiments on spray cone angle and air core diameter of hollow cone swirl rocket injector. They made 49 cold flow tests in order to find out spray cone angle and air core diameter. They stated that the injection pressure does affect both air core diameter and spray cone angle. If the injection pressure increase, spray cone angles and air core diameter increase.

A. Hussein et al. [22] made some experiments on the characteristics of hollow cone swirl sprat at various orifice diameters. They stated that the spray cone

angle and breakup length is affected by the injection pressure, higher pressures cause higher spray angles.

J. L. Santolaya et al. [23] made some experiments on the breakup of conical liquid sheets, the diameters and velocities of particles were measured by Doppler particle analyser. They revealed the diameters and velocities of droplets at different distances from hollow cone injector, and they took the spray angle 80 degrees in all experiments according to ambient conditions. According to all these spray analysis and injector characteristics, the spray angle will be taken as 80 degrees, and it will be injected from 0.3 mm diameter.

In literature, many computational studies have been done up to now. The importance of CFD analysis before manufacturing has mentioned before. Some of the correlations will be mentioned here.

Little and Manners [24], Srinivasan et al. [25], and Karki et al. [26] could be able to simulate diffuser, and secondary air channel in order to see velocity distribution in 3 dimensions. Later on, Mongia [27] claimed that these numerical calculations were not correct, than he claimed that whole geometry has to be simulated in order to see pressure loss and velocity distribution.

Lai [28] simulated a combustion chamber with swirler by using standard k-ε turbulence model and Standard Eddy-Break Up (Standard EBU). Also he could be able to simulate multiphase flow by using Lagrangian method. According to results he obtained from numerical analysis and experimental analysis they had an enough agreement.

Crocker et al. [29] simulated a combustion geometry with the solid body by using standard k-ε turbulence model and β-PDF Equilibrium combustion model. They suggested both turbulent Prandtl and Schmidth number should be 0.25 in order to have a good agreement when compared to wall temperature distribution obtained from experiments.

Smiljanovski and Brehm [30] simulated a combustion chamber manufactured by BMW, and they tried to find temperature distribution and NOx concentrations.

Malecki et al. [31] simulated a combustion chamber by using Standard k-ε turbulence model. They aimed to find the temperature distribution at the combustion chamber exit because it is so critical for turbine blades. Furthermore, they suggested both turbulent Prandtl and Schmidth number should be 0.6 in order to have a good agreement when compared to exit temperature distribution obtained from experiments. They reported that when compared to experiments, the maximum difference of the outlet temperature is just 22 K.

Di Mare et al. [32] made combustion chamber simulation by using Smagorinsky-Lilly turbulence model and β-PDF Flamelet combustion model with Large Eddy Simulation (LES). The results obtained from CFD and experiments compared, and the results showed good agreement on temperature distribution and mixture fraction. The simulation was done in transient condition, and they could succeed just 10 milliseconds of the combustion by using 64 processor computer during more than 400 hours.

Boudier et al. [33] simulated a helicopter engine by using LES with different number of meshes. They stated that the number of meshes affect the results; the number of fluctuations grow with respect to number of meshes. They also expressed that LES is not practical on the move.

Nanduri et al. [34] examined different turbulence models in Reynolds Averaged Navier-Stokes (RANS) by using Standard EBU combustion model. In the study, they used standard k-ε, Re-Normalisation Group (RNG) k- ε, realizable k- ε, and k- ω turbulence models and compared performances. According to their research, Re-Normalisation Group (RNG) k- ε, realizable k- ε turbulence

models are better than others in high swirl zones, and when compared to experimental results, good agreement was seen.

Brink et al. [35] compared Standard EBU and Hybrid EBU combustion models, and they stated that Hybrid EBU model has much more compatible results than Standard EBU model.

Celik [36] made some simulations on spray and combustion analysis of a combustion chamber in his Master's dissertation. He used both Standard EBU and Hybrid EBU, he claimed that these two methods give unrealistic results, he suggested β-PDF Flamelet should be used in combustor analysis.

The geometry which will be simulated was created by the company, and outer liner wall temperature distribution was obtained by using thermal dye and thermal couple. The experiment was done in 1.1 bar inlet pressure and 407.7 K inlet temperature, the results reported and will be compared CFD results by applying boundary conditions the same. The experiments were done by A. Topal [37].

Singh et al. [38] examined flow characteristics of an annular combustion chamber by using CFD tools (Fluent). Their geometry has 8 fuel injectors, and they simulated just one eighth of the geometry. They examined velocity, temperature, mixture fraction distributions and mass flow rates of air passing in liner holes.

A number of heat transfer simulations were done by CFX-TASCflow and CFX-5 [39] in order to compare computational results and experimental results by using different turbulence models. The report suggested that the k- ε turbulence models with scalable wall functions have much better agreement with the experimental data than results obtained from k-ω and SST models.

To simulate in multiphase is difficult, so it is suggested that Methane-air mixture can be used in order to simulate combustion by using only multi-

component gas model. Combustion is a difficult problem to solve, there are many reaction steps in combustion. Westbrook and Dryer [40] suggested 2 step-reactions for methane-air combustion. F Mauss and N. Peters [41] suggested 4 step and 9 step combustion reactions, and they compared burned gas velocities and compared the results to the experimental results. They reported that numerical results obtained by using many reaction steps have much more agreement than one-step reaction. By using many reaction steps, NO_x, O_2 concentrations were computed. By using just one-step reaction, emissions cannot be found.

Westbrook and Dryer [40] published an article about the oxidations of hydrocarbons, he suggested single-step, two-step and four-step combustion mechanisms. They also provided reaction rates which will be used while defining Standard EBU combustion models.

Boudier et al. [42] simulated a helicopter engine by using LES, they used two-step reduced mechanism. They compared to results with the other simulations which were used RANS and U-RANS. At the exit of combustion chamber, RTDF distribution was computed more heterogeneous than other methods.

1.5. Scope of This Dissertation

The scope of this dissertation is to investigate liner wall temperature distribution of an annular combustion chamber that was designed for a small turbojet engine. It is critical to be far away from the melting temperature of the solid because the properties of solid change unexpectedly, and it can cause failure. Especially while designing a small combustion chamber, the details should be considered critically. In this study, RANS method was used with different combustion models. The geometry was created by the industry (Tusas Engine Industries) and was tested in different conditions from operational conditions thought in conceptual design. The test conditions were applied to the geometry,

and the results were compared to experimental results. Then, operating conditions were applied and simulated by using STAR CCM+.

In order to investigate heat transfer and temperature distribution on the liner wall, suitable boundary layer thicknesses, the number of boundary layers and the stretching ratio between the layers. Additionally, the effect of using gas properties as constant or temperature-dependent; the effect of using the fuel as gas or liquid phase were compared.

2. COMBUSTION CHAMBER DESIGN CRITERIA AND CONCEPTUAL DESIGN

In order to design a new concept for combustion chamber, a number of criteria should be satisfied. Additionally, conceptual design and requirements are satisfied the geometry regarding boundary conditions as well as operating conditions. Many important design criteria and conceptual design parameters obtained during last century. Some of the fundamental criteria and calculations are given below.

2.1. Important Design Criteria

Pressure loss in gas turbine generally changes between 2% and 8% but in aerospace industries, it changes between 4% and 6% [7]. That was thought %5 for the design, it is suitable for also jet penetration.

The most important design requirement of combustion chamber is temperature distribution of combustion chamber outlet. Turbine mechanisms comes after combustion chamber and there are Nozzle Guide Vanes (NGV) between combustion chamber and turbine in order to arrange gas flow. Hub and tip parts of NGV are exposed to high mechanic forces. Because of that reason outlet temperature distribution is desired that temperature degrees of bottom and top zones of outlet are lower than middle zone. Although radial temperature distribution is desired also in order. In order to provide these desires, there are

two dimensionless temperature distribution factor; RTDF (Radial Temperature Distribution Factor), OTDF (Overall Temperature Distribution Factor) [7]

$$RTDF=\frac{Tmr,4 - T4}{T4 - T3} \qquad \text{Equation 1}$$

$$OTDF=\frac{Tmax,4 - T4}{T4 - T3} \qquad \text{Equation 2}$$

Expressions in the formula; $T_{mr,4}$ is the highest mean temperature of each radius of combustion chamber outlet. $T_{max,4}$ is the maximum temperature that seen at outlet, and T_4 is the mass flow averaged temperature of the CC outlet.

In combustor design RTDF value is desired between 10% and 20% and also OTDF value is desired between 15% and 45%. In the design RTDF should be 12% and OTDF should be 30% [14].

Wall temperatures of combustor are also important in design, because the temperatures of wall must be lower than melting temperature of the material. The material or design can be changed according to temperatures [13]. As a material is preferred Nickel-Cobalt compositions because of having lower densities, high melting points and higher conduction coefficients.

To reduce fuel consumption is achieved by higher pressure ratios and higher turbine entry temperatures, but those cause to raise heat transfer to liner wall from fluid by radiation. Liner holes are needed in order to reduce wall temperatures by convection with secondary air channel.

An important issue in combustor design is emissions. Higher temperatures cause NO_x, CO and HC. In order to provide emissions AFR (Air to Fuel Ratio) can be increased and also combustion should spread in the chamber. [13]

Combustor was designed smaller because of dimension limits so residence time is lower. This leads to lower combustion efficiency, in the conceptual design efficiency is thought 96%.

2.2. Conceptual Design and 1 Dimensional Modelling

There are several important criteria in 1D design in combustor, those can be put in order as [7];

- Reference velocity
- Combustor zones
- Residence Time
- Loading Factor
- Combustion Intensity

Reference velocity is a size that calculated by considering maximum combustion chamber crosscut area in cold flow. It is desired between 5 and 30 m/s [14]. In the design it can be calculated as 14.7 m/s regarding to performance analysis.

$$V_{ref} = \frac{m_{air}}{\rho_{T_3} A_{ref}}$$

Equation 3

There are three zones of combustion chamber; primary, secondary and dilution zones. It is desired that combustion should finish in primary zone, but combustion can be completed in secondary zone. High temperatures are reduced in dilution zone by dilution air, thus temperatures come suitable for NGV.

Residence time expresses duration time of a flow particle in CC and is generally about 3 milliseconds [14]. Because of having lower volume, in the design residence time is calculated as 1.23 milliseconds.

$$\tau = \frac{V_{ft}.P_{03}.10^8}{m_{air}.R.T}$$

Equation 4

In the formula V_{FT} is volume of flame tube, P_{03} is inlet pressure, T is mean gas temperature, R is gas constant and m_{air} is air mass inside of the tube.

Loading factor is an important design factor that expresses whether produced heat can be hold up by combustion chamber or not. Loading factor should be less than 10 [15]. In the design, it is calculated as 12.09. The loading factor value is very higher than required because of being too small and dimension limitations.

$$\Omega = \frac{m_{air}}{V_{ft}.{P_{03}}^{1.8}10^{\left(\frac{T_{03}}{700}\right)}} \qquad \textit{Equation 5}$$

P_{03} pressure at CC inlet and T_{03} is the mean temperature at CC inlet.

Combustion intensity expresses that the proportion of produced heat to volume. It is desired about 100 MW/m3.atm [15].

$$intensity = \frac{m_{fuel}.LHV}{P_{03}.V_{ft}} \qquad \textit{Equation 6}$$

According to performance analysis, it is calculated as 155.9 MW/m3.atm.

Table 1:1 Dimensional parameters

Parameter	Symbol	Value	Unit
Air mass flow rate	m_{air}	0,712	kg/s
Fuel mass flow rate	m_{fuel}	0,01453	kg/s
Combustor Inlet Temperature	T_{03}	478.1	K
Combustor Inlet Total Pressure	P_{03}	4.07	bar
Combustor Exit Total Pressure	P_{04}	3.86	bar
Exit Total Temperature	T_{04}	1200	K
Reference velocity	V_{ref}	14.7	m/s
Residence time	τ	1.23	ms
Loading factor	Ω	12.09	$kg/s.bar^{1.8}m^3$
Combustion intensity	-	155.9	MW/m3.atm

2.3. Adiabatic Flame Temperature Calculation

In order to compute both inner and outer side of liner wall, the flame temperature is needed to be known accurately. The flame temperature affects the liner wall temperature by convection and radiation. Because of having high orders, if temperature increases, radiation effect gets more efficient. Adiabatic flame temperature depends on fuel, inlet temperature of air and fuel-air ratio. There are some correlations on the adiabatic flame temperature depending on different fuels. [43]

As mentioned before JP-8 is a petroleum product and consists of many different molecules. Celik [36] used n-dodecane as a surrogate fuel corresponding to JP-8 in his research. In the research specific heats of gases and other important properties of gases were taken as depending on temperature.

The flame temperature changes any location inside of the flame tube. Odgers [44] suggested combustion efficiencies both in the primary and secondary zone. His formulas are given below;

In primary zone,

$$\eta_{PZ,max} = 0.72 + 0.29\ tanh[1.5475\ \cdot 10^{-3}(T_a + 108lnP_a - 1863)] \quad \textit{Equation 7}$$

In secondary zone,

$$\eta_{SZ,max} = 0.80 + 0.29\ tanh[1.5475\ \cdot 10^{-3}(T_a + 108lnP_a - 1863)] \quad \textit{Equation 8}$$

According to calculations, the maximum flame temperature is estimated to be around 2200 K.

At the combustion chamber exit, it is aimed to reach 1200 K by considering combustion efficiency as 96%.

2.4. Metal Temperature Calculations

Although thermal stresses have less impact on liner wall, it is critical that there are high temperatures in the flame tube, those cause problems when considered long life-time operations. Lefebvre [13] claimed that the liner wall temperature shouldn't exceed 1100 K, but this could be increased because of technological improvements. [13]

Liner wall temperature cooling has been important from 1950s, because higher compression ratios caused higher entry temperatures to inlet. Additionally, higher flame temperatures make radiation heat transfer from burned gases to the liner wall more efficient. Furthermore, the regulations due to environmental problems, emissions produced by aero-engines are desired to be less than some identical values. This made manufacturers and engineers to manufacture less emission produced engines. Emissions are caused by high flame temperatures. [13]

There are mainly 5 heat transfer methods seen in a combustion chamber; convection and radiation heat transfer from hot gases to the liner, conduction inside of the liner wall through the direction of heat transfer, convection and radiation heat transfer from liner to cold gases.

It is assumed that after several minutes of take-off operations, the conditions can be thought as steady, which is the liner wall reaches a stable temperature. In this case, two small elements on the liner wall surface is taken, and heat transfer analytic analysis is done on this part. The areas of the elements were symbolised as ΔA_1 and ΔA_2. R_1 and R_2 are radiation heat transfers, and C_1 and C_2 are convective heat transfers, K_1 and $K_{1\text{-}2}$ are conductions.

$$(R_1+C_1+K_1)\,\Delta A_1 = (R_2+C_2)\,\Delta A_2 = K_{1\text{-}2}\,\Delta A_2 \qquad \text{Equation 9}$$

In this formula, K_1 is the conduction heat transfer along liner wall, and it can be neglected. Additionally, the areas taken both sides of the liner can be thought as the same, $\Delta A_1 \approx \Delta A_2$.

Basically, the heat transfer equation turns to;

$$R_1+C_1= R_2+C_2=K_{1-2} \quad \textit{Equation 10}$$

In the formula conduction heat transfer inside of the liner wall is expressed by K_{1-2} and is formulated as;

$$K_{1-2}=\frac{k_w}{t_w}(T_{w1}-T_{w2}) \quad \textit{Equation 11}$$

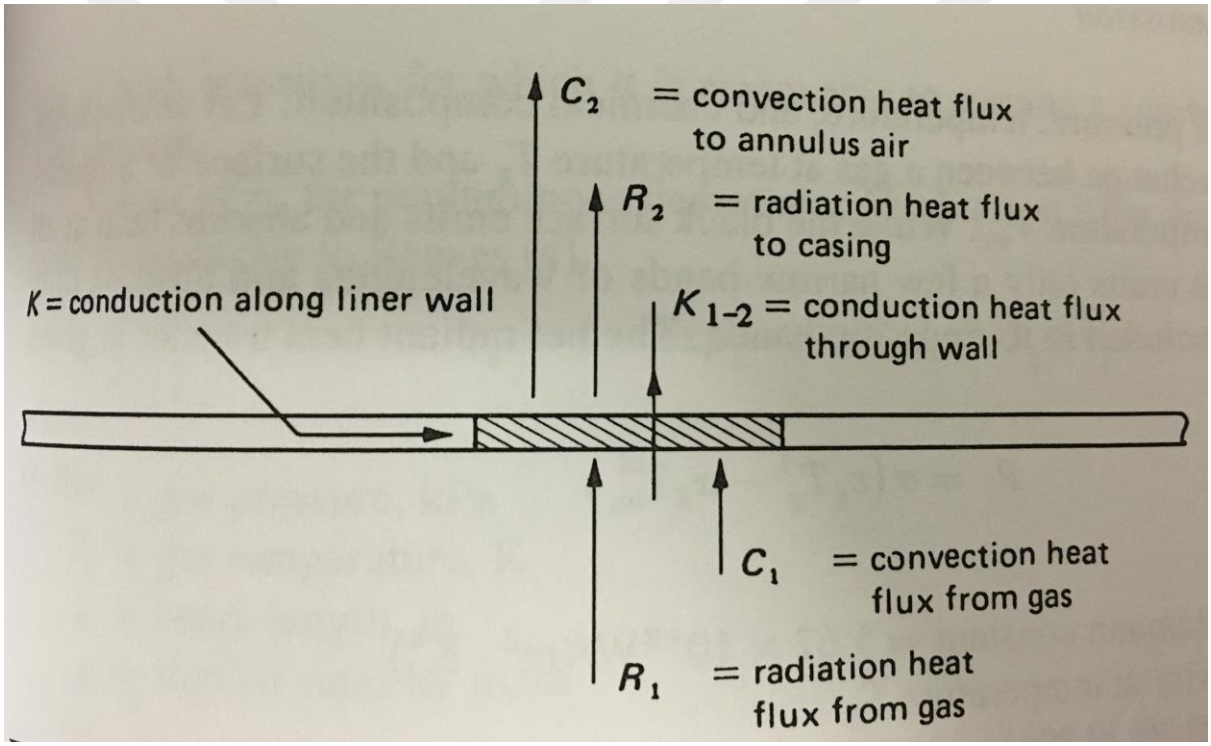

Figure 10: Conjugate heat transfer process in the liner [13]

In radiation heat transfer, temperature level is very important because the fourth power of the temperature is used, so less temperature degrees can be neglected. The heat transfer can be expressed as;

$$R_1+C_1= C_2= K_{1-2} \quad \textit{Equation 12}$$

According to Lefebvre the formulas for radiation and convective heat transfers are given below;

$$R_1 = 0.5 \cdot \sigma \cdot (1 + \varepsilon_w) \cdot \varepsilon_g \cdot {T_g}^{1.5} \cdot ({T_g}^{2.5} - {T_w}^{2.5})$$ *Equation 13*

$$C_1 = 0.020 \cdot \frac{k_g}{D_L^{0.2}} \cdot \left(\frac{m}{A_L \cdot \mu_g}\right)^{0.8} \cdot (T_g - T_w)$$ *Equation 14*

$$R_2 = \sigma \cdot \frac{\varepsilon_w \cdot \varepsilon_c}{\varepsilon_c + \varepsilon_w \cdot (1 - \varepsilon_c) \cdot (A_w/A_c)} \cdot ({T_w}^4 - {T_3}^4)$$ *Equation 15*

$$C_2 = 0.020 \cdot \frac{k_a}{D_{an}^{0.2}} \cdot \left(\frac{m}{A_{an} \cdot \mu_a}\right)^{0.8} \cdot (T_w - T_3)$$ *Equation 16*

While computing radiation heat transfer, emissivity can be calculated depending on numerous variables, and its formula is given below;

$$\varepsilon_g = 1 - exp(-290 \cdot P \cdot L \cdot (q \cdot l_b)^{0.5} \cdot T_g^{-1.5})$$ *Equation 17*

In the formula, L expresses luminous gases affect, and l_b is beam length, these terms are expressed as following;

$$L = 336/H^2$$ *Equation 18*

$$l_{b=(total\ volume|total\ surface\ area)}$$ *Equation 19*

This method was used just uncooled geometries and calculations give average results. The maximum temperature is around 1500 K.

2.5. Liner Material Properties

The liner materials should be chosen correctly in case of any failure. The properties of the metal should be suitable for the combustion conditions. Additionally, simulations will be done in take-off conditions. If the geometry is suitable for this conditions, it means it is also suitable for the cruise condition. Because the required power or thrust is maximum while taking off. If the liner wall temperature is in the safe zone in take-off conditions, it will be suitable in cruise conditions as well.

The liner wall material was selected as Inconel 625, based on Nickel (58%), Chromium (20-23%) and some other elements. The properties of the metal depend on temperature. The most important properties of the metal are thermal conductivity and melting point. Thermal conductivity should be as much as higher whereas the thickness of the liner should be as low as possible in order to increase heat transfer from hot flow region to cold flow region.in the simulations, the temperature-dependent properties were selected as given in the report prepared by the manufacturer. [45]

Some of the properties of the metal are given below.

- Nickel……...58.0%
  Chromium……..…20.0-23.0%
  Iron……..…….5.0%
  Molybdenum……..…8.0-10.0%
- Density: ……..…...8.44 g/cm3
- Melting Range ……..……...1290-1350 °C
- Thermal conductivity at 920 °C……..…23.62 W/(m.K)
- Thermal Expansion Coefficient at 920 °C…..…….. 8.96x10-6m/(m.K)

3 MATHEMATICAL MODELLING OF THE FLOW

In this chapter, the models have been used in the simulations will be mentioned. Fluid is defined as it cannot resist to external shear forces. Gases and liquids are called as fluids, and these all have similar properties in terms of governing equations; conservation of mass, conservation of momentum. These conservation and law of motion is expressed by Navier- Stokes equations.

3.1. Mathematical modelling of gas flow

3.1.1 Governing Equations

In this part, the governing equations which defines the flow will be given in Cartesian coordinates and also tensor form. First of all, in fluid flows, conservation of mass, momentum and scalars (energy, species) should be sustained for a Control Volume (CV). Conservation equations for mass, also called continuity, conservation of momentum, and conservation of any scalar value are given below.

3.1.1.1. Conservation of mass

When considered a control volume V bounded by a surface S fixed in the space, if the mass inside of the volume conserved, the total mass flux entering the geometry has to be equal to the total mass flux leaving the geometry.

Rate of decrease of mass in;

$$V = -\frac{d}{dt}\int_V \rho\, dV = -\int_V \frac{\partial \rho}{\partial t}\, dV. \qquad \textit{Equation 20}$$

Rate of mass flux out of the volume;

$$V = \int_{\mathbf{S}} \rho\, \mathbf{v} \cdot d\mathbf{S} = \int_V \nabla \cdot (\rho \mathbf{v}) dV \qquad \textit{Equation 21}$$

The integral used in the formula 21 can be expressed as;

$$\nabla \cdot (\rho \mathbf{v}) = \frac{\partial(\rho u)}{\partial x} + \frac{\partial(\rho v)}{\partial y} + \frac{\partial(\rho w)}{\partial z} \qquad \textit{Equation 22}$$

Where x, y, z are Cartesian coordinates, and u, v, w are the velocities in three orthogonal directions.

Continuity equation, conservation of mass in general form is given as following;

$$\frac{\partial \rho}{\partial t} + \nabla.(\rho v) = 0 \qquad \textit{Equation 23}$$

In the formula, ρ is the density of fluid, t is time, and v is the velocity vector.

3.1.1.2. Conservation of momentum

When considered a control volume V bounded by a surface S fixed in the space, its momentum is expressed as

$$\int_V dV \rho \, \mathbf{v} \qquad \text{Equation 24}$$

Rate of change of momentum;

$$\frac{d}{dt}\int_V dV \rho \, \mathbf{v} = \int_V dV \rho \frac{D\mathbf{v}}{Dt} \qquad \text{Equation 25}$$

This must equal the net force on the element, and total force acting on the element is given as;

$$\begin{aligned} \text{Total force (body + surface)} &= \int_V dV \rho \mathbf{g} + \int_{\mathbf{S}} [\Pi] \cdot d\mathbf{S} \\ &= \int_V dV \left(\rho \mathbf{g} + \nabla \cdot [\Pi]\right). \end{aligned} \qquad \text{Equation 26}$$

By applying Newton's second law, finally the Cauchy equation for the conservation of momentum is obtained as;

$$\rho \frac{D\mathbf{v}}{Dt} = \rho \mathbf{g} + \nabla \cdot [\Pi] \qquad \text{Equation 27}$$

In Cartesian coordinates the equation can be much more clear, and expressed in 3 directions as following;

$$\begin{aligned} \text{Momentum, } x: \ \rho \frac{Du}{Dt} &= \rho g_x + \frac{\partial}{\partial x}(\Pi_{xx}) + \frac{\partial}{\partial y}(\Pi_{xy}) + \frac{\partial}{\partial z}(\Pi_{xz}) \\ \text{Momentum, } y: \ \rho \frac{Dv}{Dt} &= \rho g_y + \frac{\partial}{\partial x}(\Pi_{yx}) + \frac{\partial}{\partial y}(\Pi_{yy}) + \frac{\partial}{\partial z}(\Pi_{yz}) \\ \text{Momentum, } z: \ \rho \frac{Dw}{Dt} &= \rho g_z + \frac{\partial}{\partial x}(\Pi_{zx}) + \frac{\partial}{\partial y}(\Pi_{zy}) + \frac{\partial}{\partial z}(\Pi_{zz}) \end{aligned} \qquad \text{Equation 28}$$

3.1.1.3 Conservation of any scalar

Conservation of any scalar (energy, species) can be expressed as the following;

$$\frac{\partial(\rho\phi)}{\partial t}+\frac{\partial(\rho u_j\phi)}{\partial x_j}=\frac{\partial}{\partial x_j}\left(\Gamma\frac{\partial\phi}{\partial x_j}\right)+q_\phi$$

Equation 29

Conservation of energy is expressed as following because reactions generate energy, enthalpy is expressed as transported scalar.

$$\frac{\partial(\rho H)}{\partial t}+\frac{\partial(\rho u_j H)}{\partial x_j}=-\frac{\partial}{\partial x_j}\left(\frac{k_g}{C_p}\frac{\partial H}{\partial x_j}\right)+S_H+S_E$$

Equation 30

In the formula, H is total enthalpy, k_g is heat conduction coefficient, C_p is specific heat, S_H is the heat generated by reactions, and S_E expresses the heat transfer between gas and liquid form of the fluid.

Total enthalpy can be expressed as following;

$$H=h+\frac{|u_j|^2}{2}$$

Equation 31

In the formula, pressure and viscous heating effect were neglected because of being too small when compared to generated heat from reactions. h is specific heat and is computed by using the following formula;

$$h=\sum_m Y_m\left(h^0_{f,m}\left(T_{ref}\right)+\int_{T_{ref}}^{T}C_{p,m}dT\right)$$

Equation 32

In the formula Y_m is the mass fraction of the molecule 'm', $h^0_{f,m}$ is the heat of formation of the molecule 'm', and T is temperature, and T_{ref} represents reference temperature.

S_H is given below, and $\omega_{r,n}$ is the speed of reaction, $v''_{m,n}$reactant is the mole fraction of the molecule 'm' in the reaction n[th], and $v'_{m,n}$ product represents is the mole fraction of the molecule 'm' in the reaction n[th].

$$S_H = \sum_n \sum_m \omega_{r,n} h^0_{f,m} \left(\upsilon''_{m,n} - \upsilon'_{m,n} \right)$$ Equation 33

Molecule transport equation is given below;

$$\frac{\partial(\rho Y_m)}{\partial t} + \frac{\partial(\rho u_j Y_m)}{\partial x_j} = -\frac{\partial}{\partial x_j}\left(\rho D \frac{\partial Y_m}{\partial x_j} \right) + S_C + S_M$$ Equation 34

In the formula, D is diffusivity coefficient of the mass, S_c is a dimensionless number called as Schmidt number, and computed as following formula.

$$Sc = \frac{\mu}{\rho D}$$ Equation 35

S_M, $S_{F,i}$ and $S_E$are liquid phase characteristics, and ω_n is a combustion term.

3.1.1.4 Navier-Stokes Equations

Navier- Stokes equations were derived by Claude-Louis Navier and George Gabriel Stokes, in order to express fluid flow, and this continuity is derived from both conservation of mass, momentum and energy. The Navier-Stokes equations in 3D is given depending on the directions for a compressible flow.

x-component:

$$\rho \cdot \left(\frac{\partial u}{\partial t} + u\frac{\partial u}{\partial x} + v\frac{\partial u}{\partial y} + w\frac{\partial u}{\partial z}\right) = \rho g_x - \frac{\partial P}{\partial x} + \frac{\partial}{\partial x}\left[2\mu\frac{\partial u}{\partial x} + \lambda div\vec{V}\right] + \frac{\partial}{\partial y}\left[\mu\left(\frac{\partial u}{\partial y} + \frac{\partial v}{\partial x}\right)\right] + \frac{\partial}{\partial z}\left[\mu\left(\frac{\partial u}{\partial z} + \frac{\partial w}{\partial x}\right)\right]$$

y-component:

$$\rho \cdot \left(\frac{\partial v}{\partial t} + u\frac{\partial v}{\partial x} + w\frac{\partial v}{\partial y} + w\frac{\partial v}{\partial z}\right) = \rho g_y - \frac{\partial P}{\partial y} + \frac{\partial}{\partial x}\left[\mu\left(\frac{\partial u}{\partial y} + \frac{\partial v}{\partial x}\right)\right] + \frac{\partial}{\partial y}\left[2\mu\frac{\partial v}{\partial y} + \lambda div\vec{V}\right] + \frac{\partial}{\partial z}\left[\mu\left(\frac{\partial v}{\partial z} + \frac{\partial w}{\partial y}\right)\right]$$

z-component:

$$\rho \cdot \left(\frac{\partial w}{\partial t} + u\frac{\partial w}{\partial x} + v\frac{\partial w}{\partial y} + w\frac{\partial w}{\partial z}\right) = \rho g_z - \frac{\partial P}{\partial z} + \frac{\partial}{\partial x}\left[\mu\left(\frac{\partial u}{\partial z} + \frac{\partial w}{\partial x}\right)\right] + \frac{\partial}{\partial y}\left[\mu\left(\frac{\partial v}{\partial z} + \frac{\partial w}{\partial y}\right)\right] + \frac{\partial}{\partial z}2\mu\frac{\partial w}{\partial y} + \lambda div\vec{V}$$

Equation 36

For an incompressible flow, $div\vec{V} = 0$ so some terms of the equations cancel out. For a steady- state flow, time derivatives cancel out.

3.1.2. Turbulence Modelling

Because of complex geometry and high velocities, the flow becomes turbulent. A flow can be described as turbulent or laminar by the evaluation of Reynolds number. The Navier- Stokes equations cannot be solved directly. In practice, it is called Direct Numerical Simulation in computational fluid dynamics, it is hard to compute by the current technology. So there are some turbulence models trying to reach real solutions. The turbulence models will be explained in this section.

Turbulent flows have eddies which can be different length scales and diffusive characteristics. Additionally, large eddies are anisotropic and depend on boundary conditions and initial conditions. [46]

Energy cascade concept was proposed by Richardson [47] in 1922, in order to define energy transfer. According to this theory, kinetic energy is transferred from large eddies to small eddies. Large eddies can transfer the energy that they store to small eddies by splitting into small eddies.

These eddies have different dimensions, and there is a scale called Kolmogorov scale. [48] He described the strength of the turbulence with the term of turbulent intensity, and this term can be described as the ratio between the root mean square of the fluctuations and the mean value and is given as the formula given below;

$$I = \frac{\sqrt{\overline{\phi'^2}}}{\bar{f}} \qquad \textit{Equation 37}$$

Where ϕ, any property, is can be split into mean and fluctuations and expressed as; $\phi = \bar{\phi} + \phi'$

The largest scale is called the length scale and is dependent on geometry, and shows the characteristics of the flow. The smallest eddy can be defined by Kolmogorov scale as following;

$$\eta_k = \left(\frac{v^3}{\varepsilon}\right)^{1/4} \qquad \textit{Equation 38}$$

$$\tau_k = \left(\frac{v}{\varepsilon}\right)^{1/2} \qquad \textit{Equation 39}$$

$$v_k = (v\varepsilon)^{1/4} \qquad \textit{Equation 40}$$

In the formulas, η_k defines Kolmogorov length scale, τ_k defines Kolmogorov time scale, v_k defines Kolmogorov velocity scale, v defines kinematic viscosity, and ε is dissipation rate of turbulent kinetic energy.

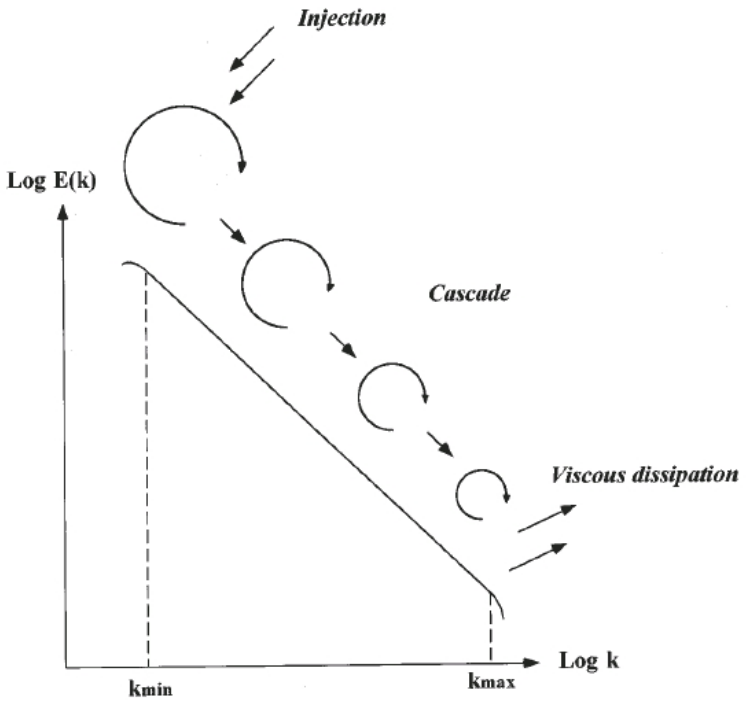

Figure 11: Energy cascade and Kolmogorov energy spectrum

To simulate whole geometry with every eddy defined according to Kolmogorov scale is possible with Direct Numerical Simulation (DNS) without any requirement to turbulence models. To simulate any flow by using DNS is too difficult in the current technology when thought about computational cells and time step. [49] DNS computes every fluctuation of the flow whereas Large Eddy Simulation (LES) computes just large eddies, and RANS models every part of turbulence assuming isotropic. To use more models to describe turbulence makes the computation time less. In LES method, the fewer eddies resolved, more computation required. For industrial applications, RANS models are very common because of being fast when compared to others, also LES can be used in both industry and academia, but DNS can be used just in some applications whose Reynolds number is small enough. [50]

In the figure 12, a comparison of LES and DNS is given in a channel flow, and figure 13 shows a sketch of velocity transition estimated by three types of simulations.

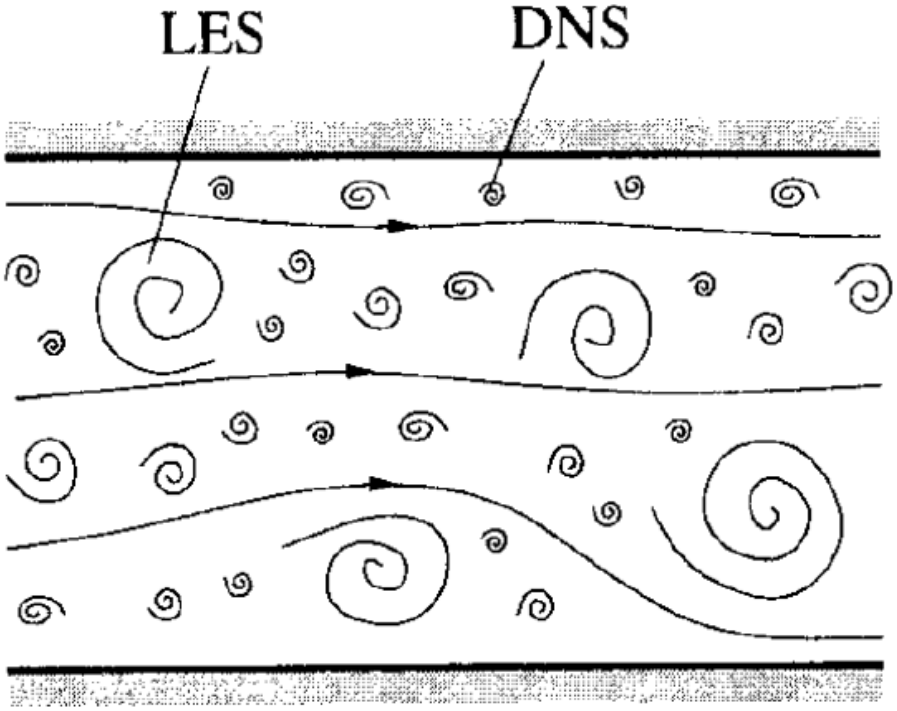

Figure 12: A schematic view of comparison between LES and DNS [51]

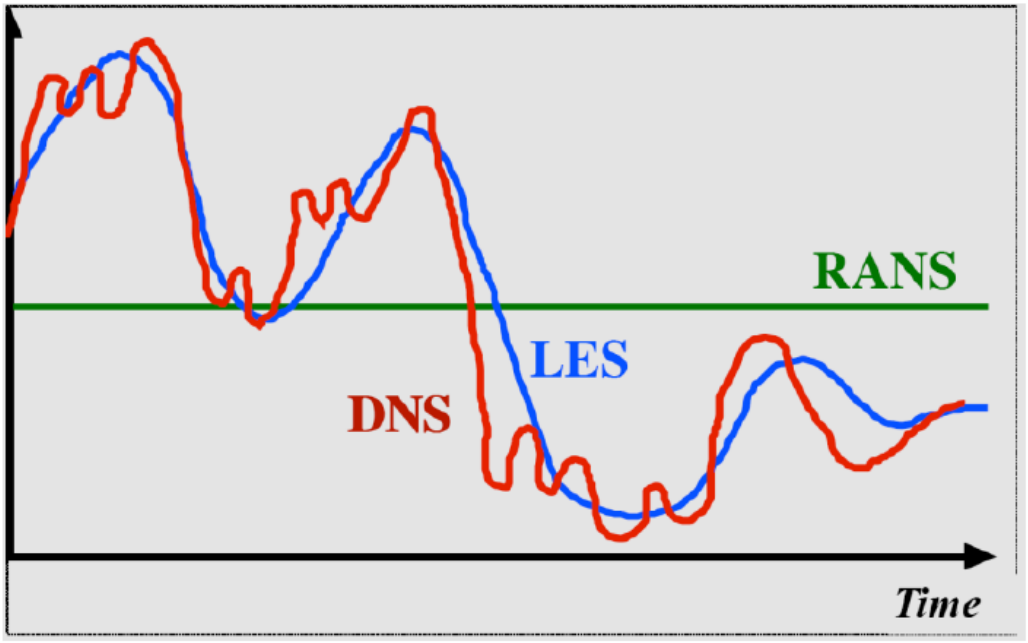

Figure 13: A sketch of velocity transition estimated by three types of models [52]

3.1.2.1 Reynolds Averaged Navier-Stokes (RANS) Simulations

This method uses basically mean values of the flow and fluctuations, continuity, momentum, energy, and molecule transport equations and can be written by Reynolds Averaging as the following [53];

$$\frac{\partial \overline{\rho}}{\partial t} + \frac{\partial}{\partial x_j}(\overline{\rho}\tilde{u}_j) = \overline{S}_M \qquad \text{Equation 41}$$

$$\frac{\partial(\overline{\rho}\tilde{u}_i)}{\partial t} + \frac{\partial}{\partial x_j}\left(\overline{\rho}\tilde{u}_j\tilde{u}_i\right) = -\frac{\partial \overline{p}}{\partial x_i} + \frac{\partial}{\partial x_j}\left(\overline{\tau}_{ij} + \widetilde{\overline{\rho}u_j^{"}u_i^{"}}\right) + \overline{S}_{F,i} \qquad \text{Equation 42}$$

$$\frac{\partial(\overline{\rho}\tilde{H})}{\partial t} + \frac{\partial(\overline{\rho}\tilde{u}_j\tilde{H})}{\partial x_j} = -\frac{\partial}{\partial x_j}\left(\overline{\rho}\alpha\frac{\partial \tilde{H}}{\partial x_j} + \widetilde{\overline{\rho}u_j^{"}H^{"}}\right) + \overline{S}_H + \overline{S}_E \qquad \text{Equation 43}$$

$$\frac{\partial(\overline{\rho}\tilde{Y}_m)}{\partial t} + \frac{\partial(\overline{\rho}\tilde{u}_j\tilde{Y}_m)}{\partial x_j} = -\frac{\partial}{\partial x_j}\left(\overline{\rho}D\frac{\partial \tilde{Y}_m}{\partial x_j} + \widetilde{\overline{\rho}u_j^{"}Y_m^{"}}\right) + \overline{S}_C + \overline{S}_M \qquad \text{Equation 44}$$

In the formulas α is the thermal diffusivity of the gas phase and expressed as;

$$\alpha = \frac{k}{\overline{\rho}C_p} \qquad \text{Equation 45}$$

The terms used in the formulas written by using Reynolds Averaging method should be modelled. In order to compute these terms, a lot of numerical methods were used. Jones and Launder [54] developed Standard k-ε model, Shih [55] et al. developed Realisable k-ε model by modifying the Standard k-ε model, and Wilcox [56] developed k-ω model.

3.1.2.1.1. Standard k-ε Turbulence Model

Standard turbulence model uses turbulent viscosity, μ_t by using an empiric constant, C_μ, as following;

$$\mu_t = \overline{\rho}C_\mu\frac{k^2}{\varepsilon} \qquad \text{Equation 46}$$

Where k is turbulent kinetic energy, and ε is the dissipation of turbulent kinetic energy, these two terms are computed by using these two formulas;

$$\frac{\partial(\bar{\rho}k)}{\partial t}+\frac{\partial}{\partial x_j}\left(\bar{\rho}\tilde{u}_j k\right)=\frac{\partial}{\partial x_j}\left(\left(\mu+\frac{\mu_t}{\sigma_k}\right)\frac{\partial k}{\partial x_j}\right)+P-\bar{\rho}\varepsilon \quad \text{Equation 47}$$

$$\frac{\partial(\bar{\rho}\varepsilon)}{\partial t}+\frac{\partial}{\partial x_j}\left(\bar{\rho}\tilde{u}_j \varepsilon\right)=\frac{\partial}{\partial x_j}\left(\left(\mu+\frac{\mu_t}{\sigma_\varepsilon}\right)\frac{\partial \varepsilon}{\partial x_j}\right)+C_{\varepsilon 1}\frac{\varepsilon}{k}P-C_{\varepsilon 2}\bar{\rho}\frac{\varepsilon^2}{k} \quad \text{Equation 48}$$

$$P=\mu_t\left(\frac{\partial \tilde{u}_i}{\partial x_j}+\frac{\partial \tilde{u}_j}{\partial x_i}\right)\frac{\partial \tilde{u}_i}{\partial x_j} \quad \text{Equation 49}$$

In the formula σ_k ,σ_ε, $C_{\varepsilon 1}$ and $C_{\varepsilon 2}$are empirical constants, and P defines the production rate of turbulence kinetic energy. The constants are given in the table 2.

Table 2: Empirical constants used in Standard k-ε turbulence model [57]

Parameter	$C_{\varepsilon 1}$	$C_{\varepsilon 2}$	C_{μ}	σ_k	σ_ε
value	1.44	1.92	0.09	1.0	1.3

3.1.2.1.2 Realizable k-ε Turbulence Model

The difference between Standard k- ε turbulence model and Realizable k-ε turbulence model is that C_{μ} and $C_{\varepsilon 1}$ parameters are calculated considering of strain rate and vorticity.

$$C_\mu=\left(A_0+A_s V^*\frac{k}{\varepsilon}\right)^{-1} \quad \text{Equation 50}$$

$$A_s=\sqrt{6}\cos\left(\frac{1}{3}\cos^{-1}\left(\sqrt{6}\frac{S_{ij}S_{jk}S_{ki}}{\left|S_{ij}\right|^3}\right)\right) \quad \text{Equation 51}$$

$$V^*=\left(S_{ij}S_{ij}+W_{ij}W_{ij}\right)^{0.5} \quad \text{Equation 52}$$

$$S_{ij}=\frac{1}{2}\left(\frac{\partial \tilde{u}_i}{\partial x_j}+\frac{\partial \tilde{u}_j}{\partial x_i}\right) \quad \text{Equation 53}$$

$$W_{ij} = \frac{1}{2}\left(\frac{\partial \tilde{u}_i}{\partial x_j} - \frac{\partial \tilde{u}_j}{\partial x_i}\right)$$ *Equation 54*

$$C_{\varepsilon 1} = max\left(0.43, \frac{\eta_\varepsilon}{5+\eta_\varepsilon}\right)$$ *Equation 55*

$$\eta_\varepsilon = \frac{|S_{ij}|k}{\varepsilon}$$ *Equation 56*

This model defines the flow better than standard model in separated regions and near wall treatment by using two layer all y+ method. [57] The parameters used in the model are given in the table 3 below.

Table 3: Empirical constants used in Realizable k-ε Turbulence Model [57]

Parameter	$C_{\varepsilon 2}$	σ_k	σ_ε	A_0
value	1.9	1.0	1.2	4.0

3.1.2.2 Large Eddy Simulation (LES)

This approach suggests to simulate the flow by regarding the large eddies inside of the flow. In this approach, a cut-off wave number is determined, and scales higher than this number are modelled. This model gives better results in terms of combustion chamber flows because the flow in the combustion chamber has instabilities and vorticities. Additionally, this model is not common in the industry, but in the future, it will play an important role of designing combustion chambers.

3.1.2.3 Detached Eddy Simulation (DES)

This approach can be defined as a hybrid model of RANS and LES. To solve near wall treatments by using LES is too difficult and takes too much computation time, so this approach suggests to use RANS model near wall and to use LES model in the rest of fluid domain. This approach gives better solutions when compared to RANS and solves the simulation quicker than LES.

3.1.2.4 Direct Numerical Simulation (DNS)

Solving Navier-Stokes equations for a flow is a way of solving turbulence. Many approaches have errors when compared to experimental values, this approach, DNS, gives most accurate results. This approach suggests to simulate even small eddies. The smallest eddies should be put at least two grid points. The turnover time of the smallest eddy must be greater than the size of a time step. This approach is too expensive to apply, and on the move, is used only for academic research. It is used only the Reynolds number level is under 10000. [50]

3.1.3 Combustion Modelling

In combustion modelling, there are types of combustion, and these are; non-premixed, partially premixed, and premixed. While Spark Engines uses premixed combustion model, in most aero engine design non-premixed, and partially premixed models are widely used. In the combustion chamber designed by Tusas Engine Industries, non-premixed combustion chamber is used. That is, the fuel and the air are injected into combustion chamber individually.

Mainly, there is two approaches in non-premixed combustion, one is finite rate chemistry, and the other one is infinitely fast chemistry. Finite rate chemistry model asserts chemical reactions happen slowly than the turbulent mixing of the air and the fuel. The infinitely rate chemistry model claims that chemical reactions happens quicker than the turbulent mixing of the air and the fuel. This parameter is defined by Damkohler number and obtained from the ratio between these two velocities. [58]

In the simulations, Standard Eddy Break up and Presumed Probability Density Function models were used and compared.

3.1.3.1 Standard Eddy Break up (EBU) Combustion Model

This finite rate chemistry model was suggested by Spalding [59], in 1970. This model claims that unburned air-fuel mixture divides by time because of interaction between burned air-fuel mixtures.

$$\tilde{\omega}_r^{mix} = -\frac{\bar{\rho}}{M_F}\frac{\varepsilon}{k}A_{EBU}\min\left(\tilde{y}_F, \frac{\tilde{y}_O}{s_O}\right) \qquad \text{Equation 57}$$

$$s_O = \frac{\upsilon_O M_O}{\upsilon_F M_F} \qquad \text{Equation 58}$$

In the formulas, $\tilde{\omega}_r^{mix}$is the speed of reaction, A_{EBU} is an empirical constant, $\tilde{y}_F$ is the mass fraction of the fuel, $\tilde{y}_O$ is mass fraction of oxidizer, v_O is the stoichiometric coefficient of the oxidizer, v_F is the stoichiometric coefficient of the fuel, M_O is the molecular weight of the oxidizer, and M_F is the molecular weight of the fuel. In the model A_{EBU} is a constant and is 4.0.

There are many reactions happened in the combustion chamber. As stated before, the fuel of kerosene or JP-8 has many components of different hydrocarbons. Celik [36] used n-dodecane ($C_{12}H_{26}$) as a surrogate fuel corresponding to real fuel. Westbrook and Dryer [40] suggested that methane (CH_4) can be used by considering the same generated energy by the reactions, and they suggested two-step reactions as following;

$$CH_4 + 1.5O_2 \rightarrow CO + 2H_2O$$

$$CO + 0.5O_2 \rightarrow CO_2 \qquad \text{Equation 59}$$

Hautman et al. [60] suggested four-step reduced reaction mechanism as following;

$$C_{12}H_{26} \rightarrow 6C_2H_4 + H_2$$

$$C_2H_4 + O_2 \rightarrow 2CO + 2H_2$$

$$H_2 + 0.5O_2 \rightarrow H_2O$$

$$CO + 0.5O_2 \rightarrow CO_2$$ *Equation 60*

Star CCM+ suggests $C_{12}H_{23}$ as a surrogate fuel for kerosene or JP-8. [57] The reaction was selected in only for one-step reaction as following;

$$C_{12}H_{23} + 17.75O_2 \rightarrow 12CO_2 + 11.5H_2O$$ *Equation 61*

The coefficients that determine the speed of reaction were suggested by Westbrook and Dryer [40], as 0.25 for $C_{12}H_{23}$ and 1.0 for O_2.

3.1.3.2 Presumed Probability Density Function (PPDF) Combustion Model

This model uses mixture fractions of fuel and oxidizer, and their variances instead of transporting every information of the mixture. Mixture fraction is defined as following, and the terms used in the formulas will be explained later;

$$z = \frac{\phi}{r+\phi}$$ *Equation 62*

$$\phi F + rO \rightarrow (\phi + r)P$$ *Equation 63*

Where ϕ is the equivalence ratio, F is fuel mass fraction, O is oxidizer mass fraction, and P symbolizes products.

A number of formulations are used in the PPDF model, and the formulas are given below [57];

The mixture fraction can consist by its mean and its variance as following;

$$z = \tilde{z} + \widetilde{z''^2}$$ *Equation 64*

The classical gradient transport closure for turbulent fluxes are formulated as;

$$\bar{\rho}\frac{\partial \tilde{z}}{\partial t} + \bar{\rho}\tilde{\boldsymbol{u}} \cdot \nabla \tilde{z} = \nabla \cdot \left(\bar{\rho} v_t \nabla \tilde{Z}\right) \quad \text{Equation 65}$$

For variance,

$$\bar{\rho}\frac{\partial \widetilde{z''^2}}{\partial t} + \bar{\rho}\tilde{\boldsymbol{u}} \cdot \nabla \widetilde{z''^2} = \nabla \cdot \left(\bar{\rho} v_t \nabla \widetilde{z''^2}\right) + 2\bar{\rho} v_t |\nabla \tilde{z}|^2 - 2\bar{\rho}\tilde{\boldsymbol{\chi}} \quad \text{Equation 66}$$

The scalar dissipation rate is defined as;

$$\bar{\rho}\tilde{\boldsymbol{\chi}} = 2\overline{\rho D \frac{\partial z}{\partial x_\iota}\frac{\partial z}{\partial x_\iota}} \quad \text{Equation 67}$$

The linear relaxation model for the balance is given as;

$$\tilde{\boldsymbol{\chi}} = \frac{\widetilde{z''^2}}{\left(k/\varepsilon\right)} \quad \text{Equation 68}$$

The closed form of the mixture fraction variance equation turns to;

$$\frac{\partial \bar{\rho}\widetilde{z''^2}}{\partial t} + \frac{\partial}{\partial x_i}\left(\bar{\rho}\tilde{u}_i \widetilde{z''^2}\right) = \frac{\partial}{\partial x_i}\left(\frac{\mu_t}{\sigma_t}\frac{\partial \widetilde{z''^2}}{\partial x_i}\right) + C_g \mu_t \frac{\partial \tilde{z}}{\partial x_i}\frac{\partial \tilde{z}}{\partial x_i} - C_d \bar{\rho}\frac{\varepsilon}{k}\widetilde{z''^2} \quad \text{Equation 69}$$

Libby and Williams [61] modified the PDF equations by suggesting the presumed function as following;

$$\tilde{P}\left(z^*; \underline{x}, t\right) = \frac{z^{*a-1}(1-z^*)^{b-1}}{\int_0^1 z^{+a-1}(1-z^+)^{b-1}dz^+} \quad \text{Equation 70}$$

$$a = \tilde{z}\left(\frac{\tilde{z}(1-\tilde{z})}{\widetilde{z''^2}} - 1\right) \geq 0 \quad \text{Equation 71}$$

$$b = a\left(\frac{1}{\tilde{z}} - 1\right) \geq 0 \quad \text{Equation 72}$$

The PPDF model has some assumptions as following;

- Mach numbers are small than 1
- The thermodynamic pressure is constant
- Lewis numbers are equal
- Turbulence level is very high

3.2 Mathematical Modelling of Liquid Flow

Combustion can only happen in gas phase, there is no combustion in liquid or solid form. A number of parameters can affect the combustion process of a liquid fuel. Because of non-realistic results obtained by using fuel in gas phase, to simulate the combustion by using fuel in liquid phase is required. There are some different spray and atomisation models called as Linearized Instability Sheet Analysis (LISA) [62], Taylor Analogy Break-up (TAB) [63], Bai-Gosman Spray-Wall Interaction [64], and Foucart Wall Film [65] models. In the simulations, LISA model was used.

3.2.1 Fundamental Equations

The droplets were modelled by the Lagrangian multiphase approach. Momentum equilibrium for droplets can be expressed as following,

$$m_p u_p = \vec{F}_D + \vec{F}_{pr} \qquad \textit{Equation 73}$$

$$\vec{F}_D = \frac{1}{2} C_d \rho A_p |\vec{u}_s| \vec{u}_s \qquad \textit{Equation 74}$$

$$\vec{F}_{pr} = -V_p \nabla p \qquad \textit{Equation 75}$$

In the formulas, C_d is friction coefficient, A_p is the surface area of the droplet, $\vec{u}_s$ is the velocity difference between the gas and liquid phase of the droplet, V_p is the volume of the droplet, ∇p is the static pressure gradient. $\vec{F}_D$ is the friction force on the droplet and $\vec{F}_{pr}$ represents the pressure on the droplet.

The energy equilibrium can be written as following;

$$m_p c_p \frac{dT_p}{dt} = \dot{Q}_{convection} + \dot{Q}_{evaporation} \qquad \textit{Equation 76}$$

In the energy formula, m_p is the mass of the droplet, c_p is the specific heat, T_p is the temperature of the droplet, $\dot{Q}_{convection}$ is the heat transfer from gases to the liquid droplet, $\dot{Q}_{evaporation}$ is the heat taken from gases to be evaporated.

3.2.2 LISA Atomisation Model

There are many models used in multiphase flows, LISA model was selected in the simulations. LISA model suggest a hollow cone injector to inject the fuel to the inside of the combustion chamber. This approach has a number of formulations like continuity, liquid film velocity, Weber numbers, and so on.

In the simulations, inner and outer cone angles, the diameter distribution of the droplets, velocities of the droplets, and injector diameter were determined according to Hamid [22] and Santolaya [23], they did a lot of experimental studies depending on injection pressure and ambient pressure.

In the simulation, considering the ambient pressure and the injection pressure, the injector diameter was selected as 0.3 mm, inner cone angle was 0.0 degree, outer cone angle was 80.0 degrees, the particle diameters were selected as 20 micrometres, and the velocities of the droplets were determined as 4 m/s. Mass flow rate and particle temperature were entered as given boundary conditions.

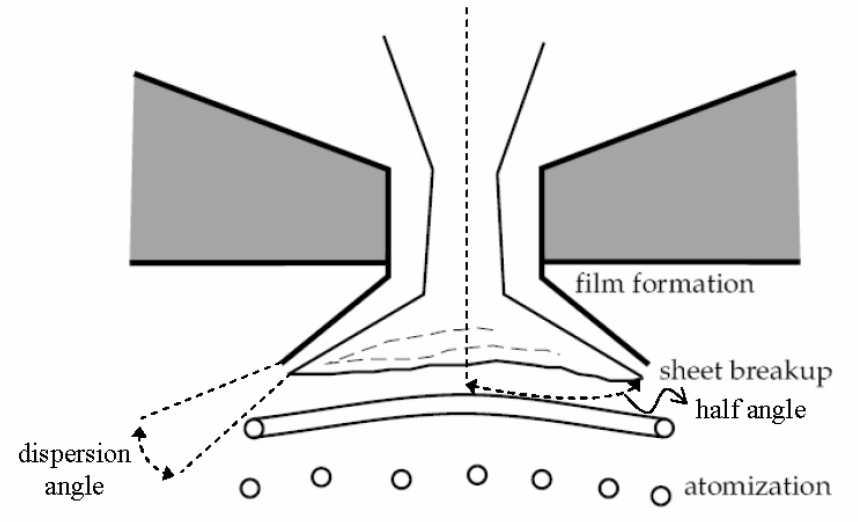

Figure 14: Theoretical Progression from the Internal Atomizer Flow to the External Spray [66]

4. COMPUTATIONAL FLUID DYNAMICS RESULTS

The geometry was designed by Tusas Engine Industries according to one-dimensional methodology and conceptual design criteria. The geometry has 7 fuel injectors which were played symmetrically. Additionally, the liner holes were opened symmetrically on the liner wall. In order to use CPU facilities efficient, one seventh of the geometry was simulated by using symmetric options of the geometry.

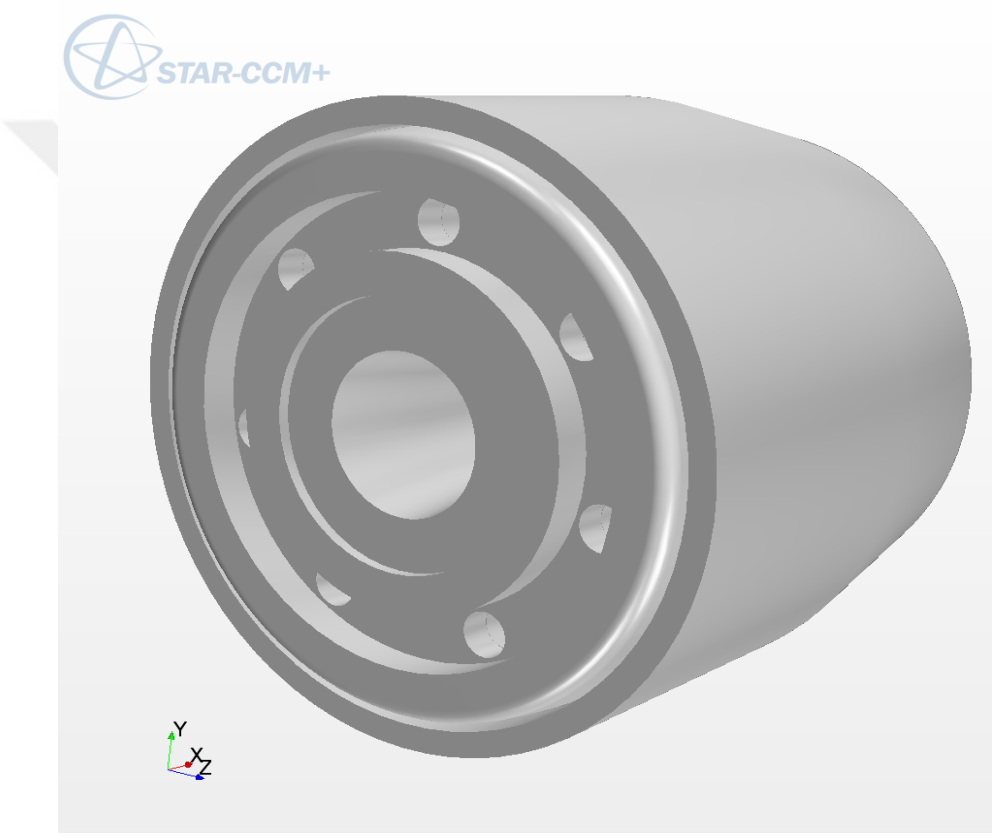

Figure 15: Full geometry view

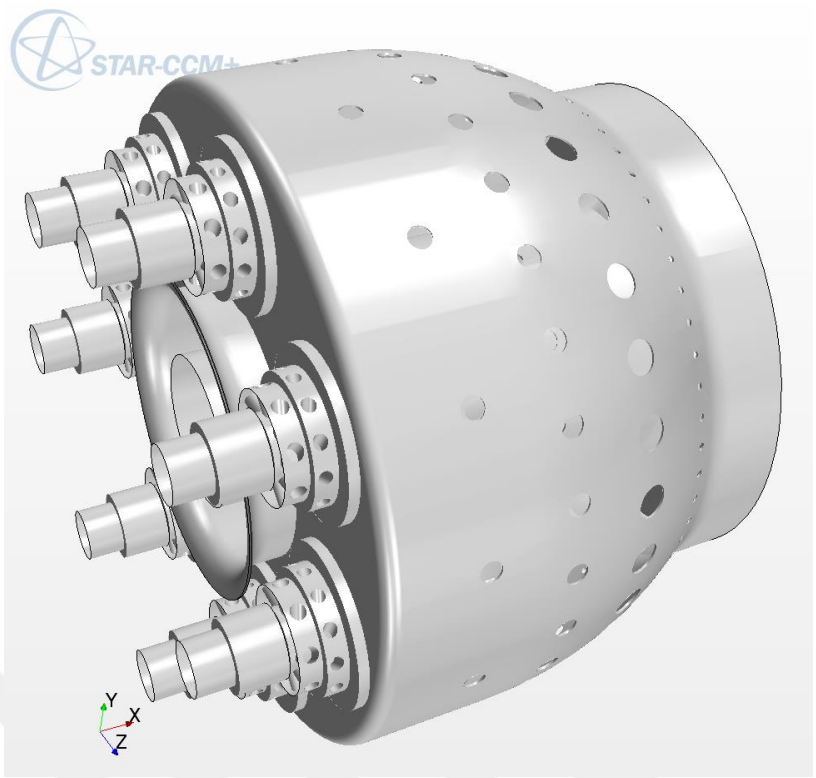

Figure 16: Full geometry view without casing

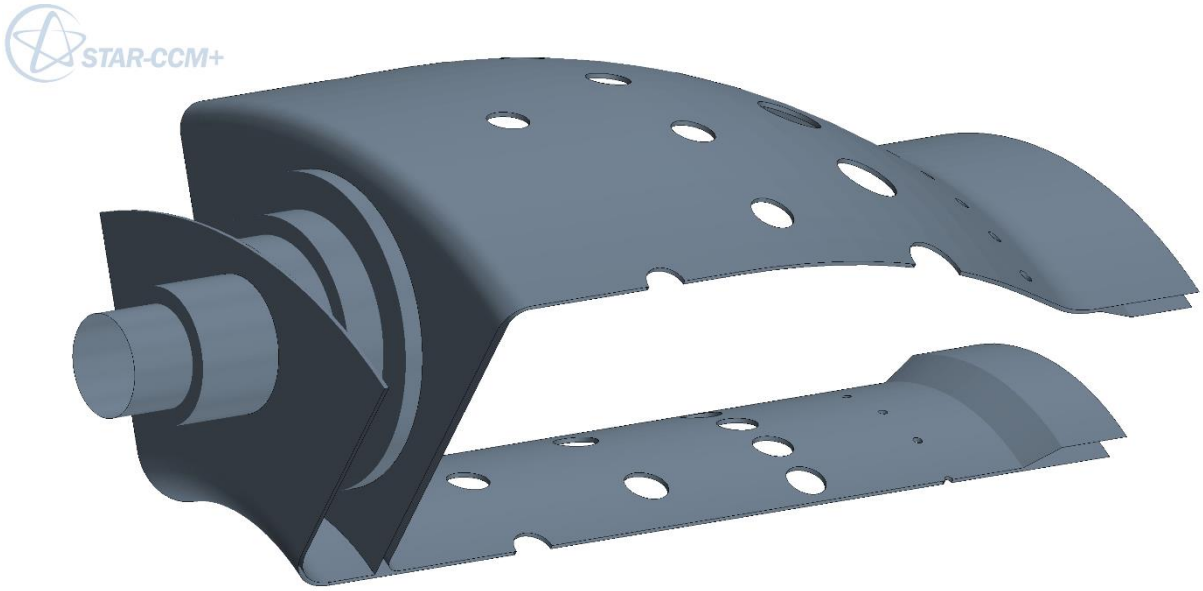

Figure 17: One-seventh of the geometry which will be simulated

The geometry was created and tested by the company. Liner wall temperature were measured by thermo-couple and thermal dye. This was reported by A. Topal [37], and in the report it is stated that the highest temperature on the liner wall was measured as 1123 K. Liner wall temperature was 969 K in average.

The boundary conditions of the experiment were different from real operation conditions. In my study, I simulated one seventh of the geometry by using different type of combustion models, by using the same number of boundary layers, same thickness and same stretching.

In the literature review, the significance of turbulence models in combustion chamber analysis is mentioned. According to simulations compared to experimental measurements, realizable k-ε model is strongly recommended for the combustion chamber, so in all simulations, this model was used.

In this study, a number of comparisons affecting the wall temperature have been done. First of all, the mesh study was worked on the simulation. The number of mesh does really affect the results, it is stated that 900000 hexahedral grid elements is enough to be on the safe side, by Schneider [67]. In the studies by creating 500000, 1100000 and 2400000 polyhedral meshes; the same simulations were done and the temperature and velocity distribution were examined in the plane section, and the measurements of temperature and velocity of some selected points were compared.

Secondly, in the beginning the fuel was selected as gas and gas properties were selected as constant, then selected as depending on temperature. As a result, the properties of gases depending on temperature affect the temperature distribution on both solid and fluid body. By using constant values and temperature dependant values were compared.

Third comparison is based on these of fuel in the liquid or gas phase. Using the fuel in the liquid phase greatly affected the simulations. The most important differences to have greatly varied results are the evaporation of liquid and having different densities.

Fourth comparison is based on combustion models. Different types of combustion models were examined by applying test boundary conditions and

initial values to the geometry with the same mesh and the other parameters. It is stated by Celik [36], standard EBU models overestimates the temperature, and also Star CCM+ conference notes stated the same when the results obtained from Standard EBU and Presumed PDF simulations to experimental measurements. In this part, Standard EBU and PPDF combustion models are compared. This comparison was done by using both test conditions and real operation conditions.

Fifth comparison is about the number of thin layer meshes inside of the solid. The number of thin layer meshes were examined whether they affect the temperature distribution or not. Thin layer meshes are used to mesh the solid body, through from the heat transfer, the direction from hot gases to cold gases. The number of thin layer meshes were selected as 3 and 4 to compare by using Presumed PDF combustion model, without changing fluid domain meshes.

Sixth comparison is about the effect of the number of boundary layers at the same thickness. In order to have reasonable wall temperature, enough number of boundary layers should be used. Star CCM+ conference notes suggest to use between 10-20 boundary layers. [57] In the simulations, by using 5, 10, 15 and 20 boundary layers were used and compared to the experimental setup results. The stretch ratio is suggested to be between 1.2 and 1.5. [57] In the simulations in this part, the stretch factor was used 1.2.

Seventh comparison is to see the effect of boundary layer stretching factor. Stretching factor defines the ratio of thicknesses of two neighbour layers. In the simulations, by using 10 boundary layers, different total boundary layer thicknesses are used by selecting the stretch ratio as 1 and 1.2. The results obtained from simulations and experimental data will be compared.

As a result, the most suitable boundary layer thickness, the number of boundary layers, and the number of thin meshes will be applied to the one seventh of the geometry with the best combustion model.

4.1 Mesh Studies

By establishing three mesh configurations via using polyhedral meshing properties, these three mesh configurations were compared to understand that the simulations are non-dependant from the number of meshes used. It is stated by Schneider [67] the simulations which used more than 900000 hexahedral meshes give realistic results, and the temperature-velocity distribution is so similar to each other. In this part, the same geometry was simulated by using three different number of meshes. The number of meshes are approximately 500000, 1100000, and 2400000 respectively.

After giving the mesh scene, temperature and scalar velocity distribution on the main plane, the velocities and temperatures of 7 points selected inside of the combustion chamber were compared to see how similar the results. The results taken from simulations were under convergence criteria.

One seventh of the geometry was simulated by using polyhedral mesh which was suggested by user guide [57]. In the simulations, the models used for turbulence and combustion are the same. Three different numbers of meshes geometry were simulated, and some of the most important results were compared. All three simulations have similar results, as suggested by Schneider [57], more than 900000 hexahedral meshes have reasonable results.

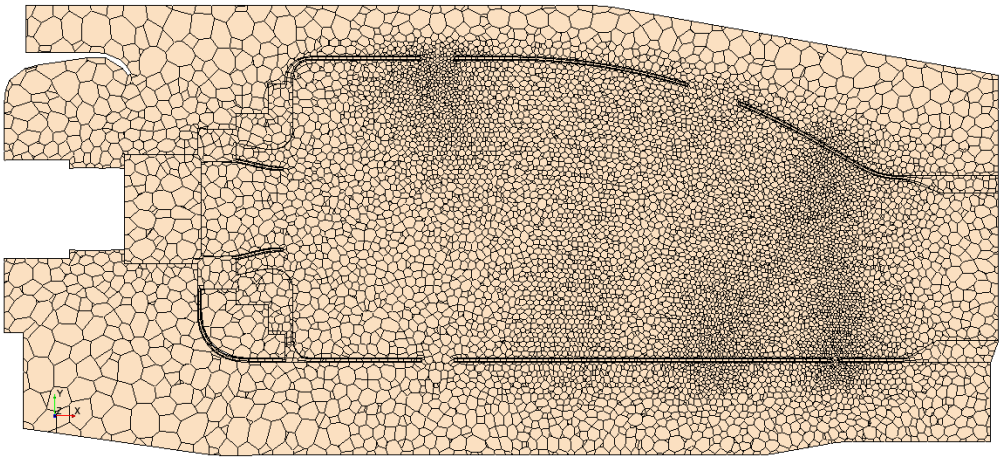

Figure 18: Mesh appearances on the main plane of mesh studies; 500000.

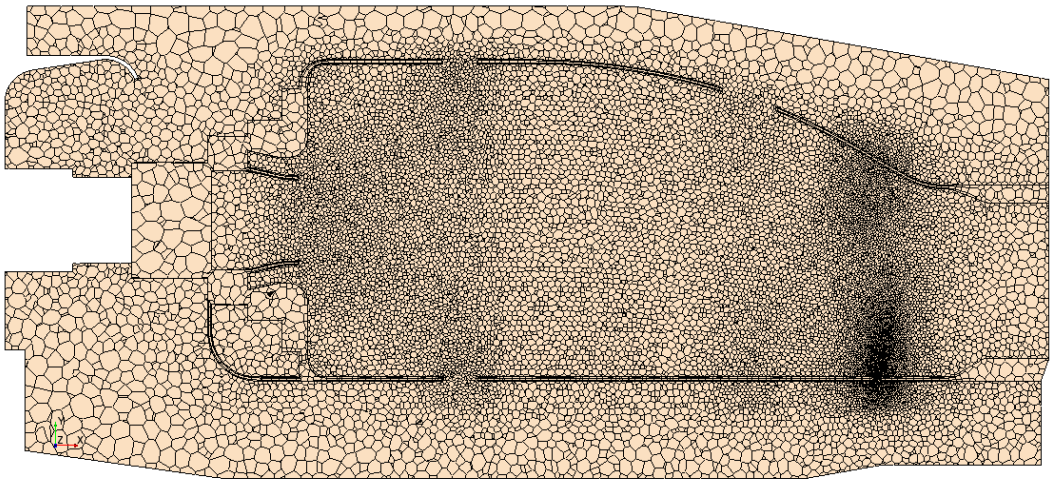

Figure 19: Mesh appearances on the main plane of mesh studies, 1100000.

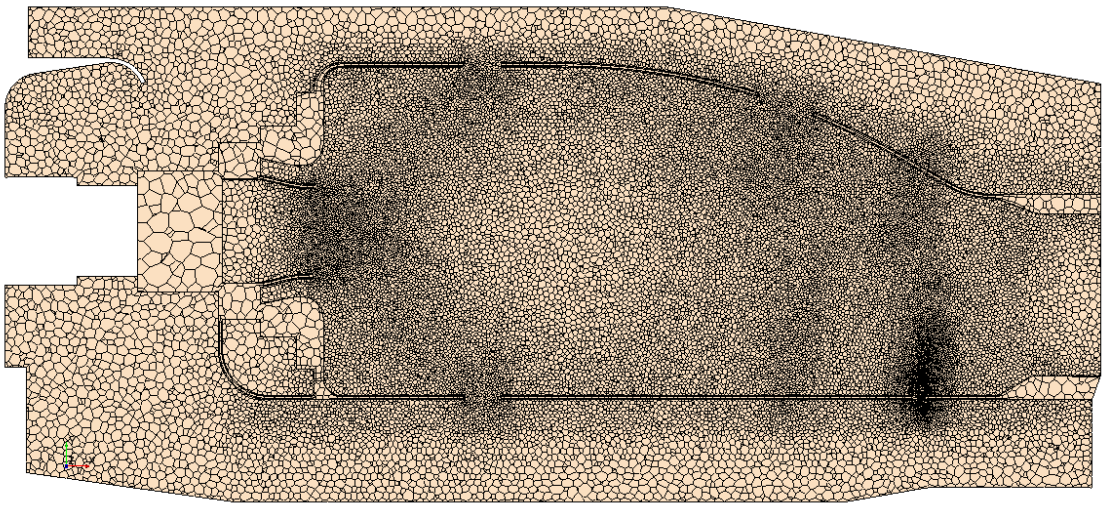

Figure 20: Mesh appearances on the main plane of mesh studies; 2400000.

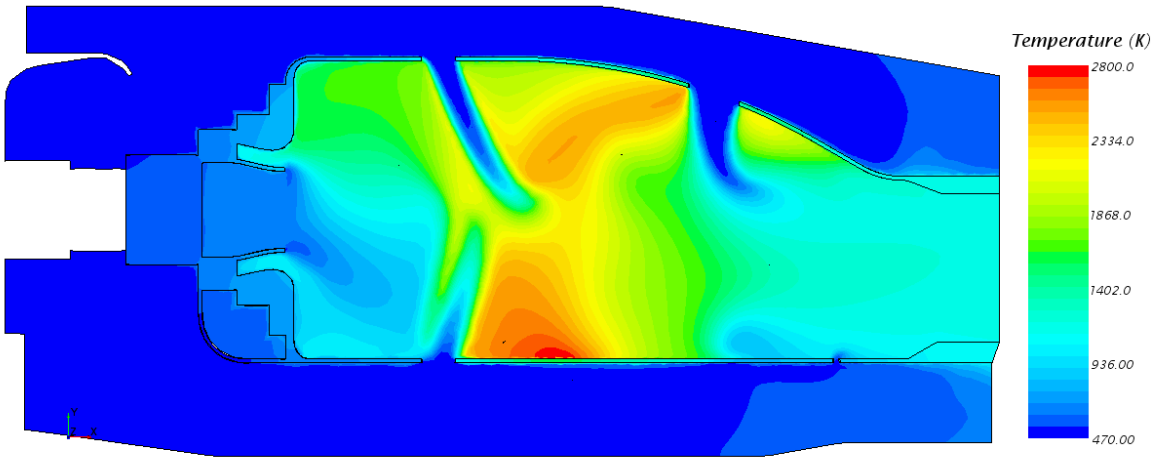

Figure 21: Temperature distribution on the main plane of mesh studies; 500000.

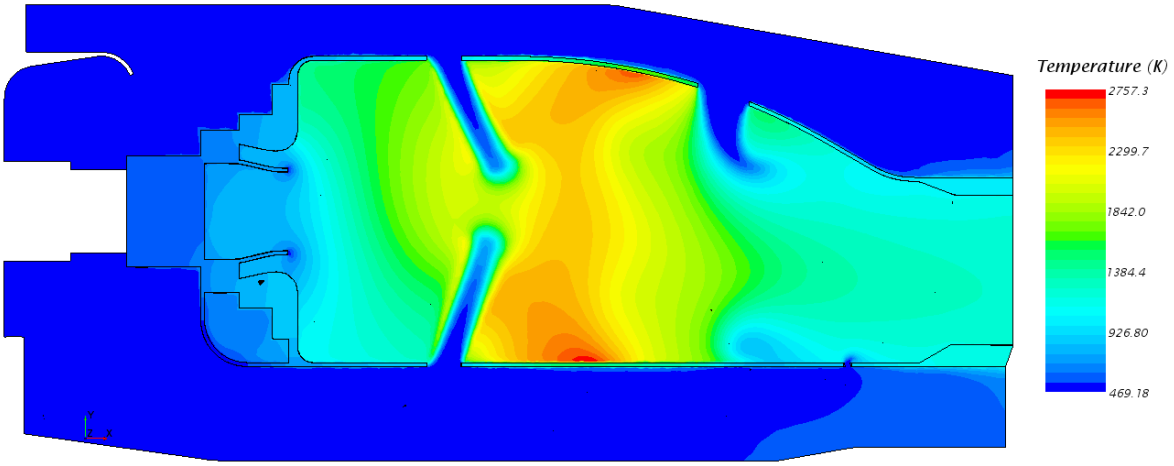

Figure 22: Temperature distribution on the main plane of mesh studies; 1100000.

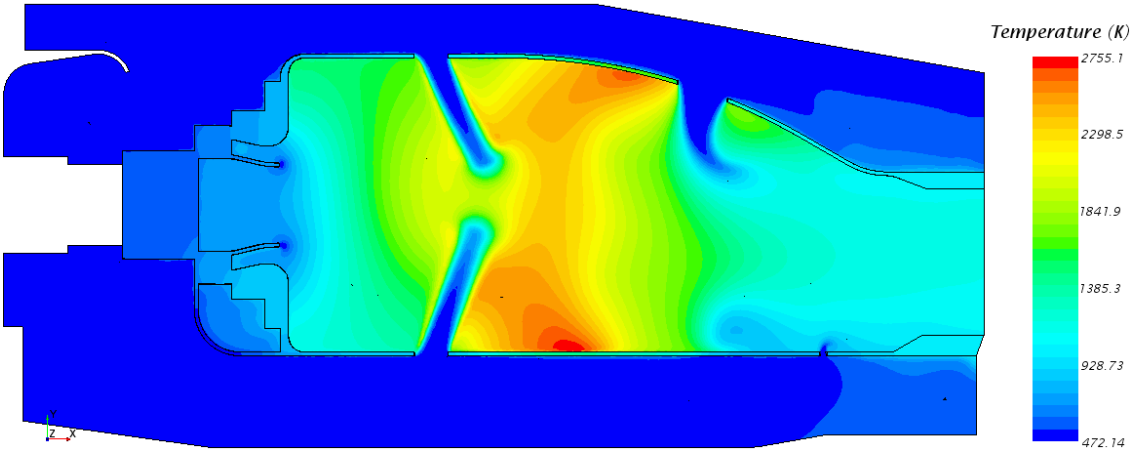

Figure 23: Temperature distribution on the main plane of mesh studies; 2400000.

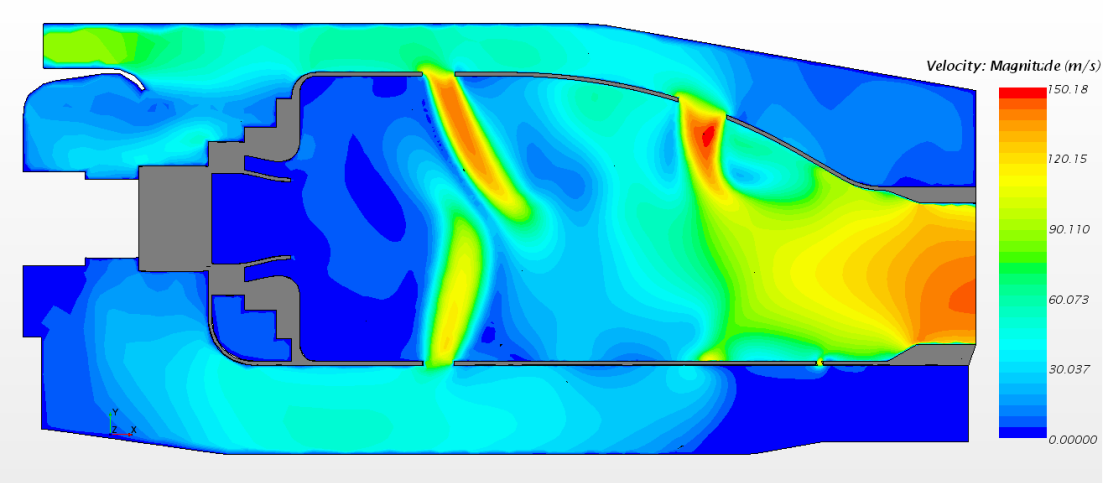

Figure 24: Velocity magnitude distribution on the main plane of mesh studies; 500000.

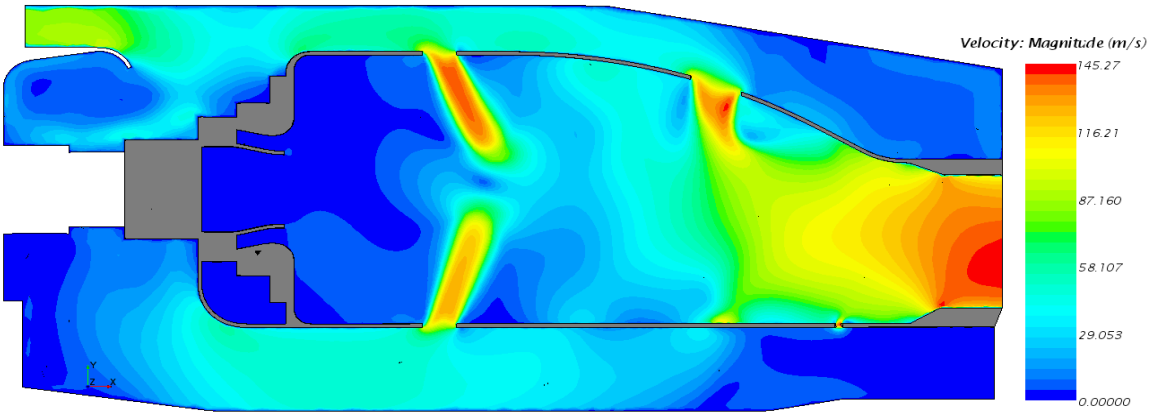

Figure 25: Velocity magnitude distribution on the main plane of mesh studies; 1100000.

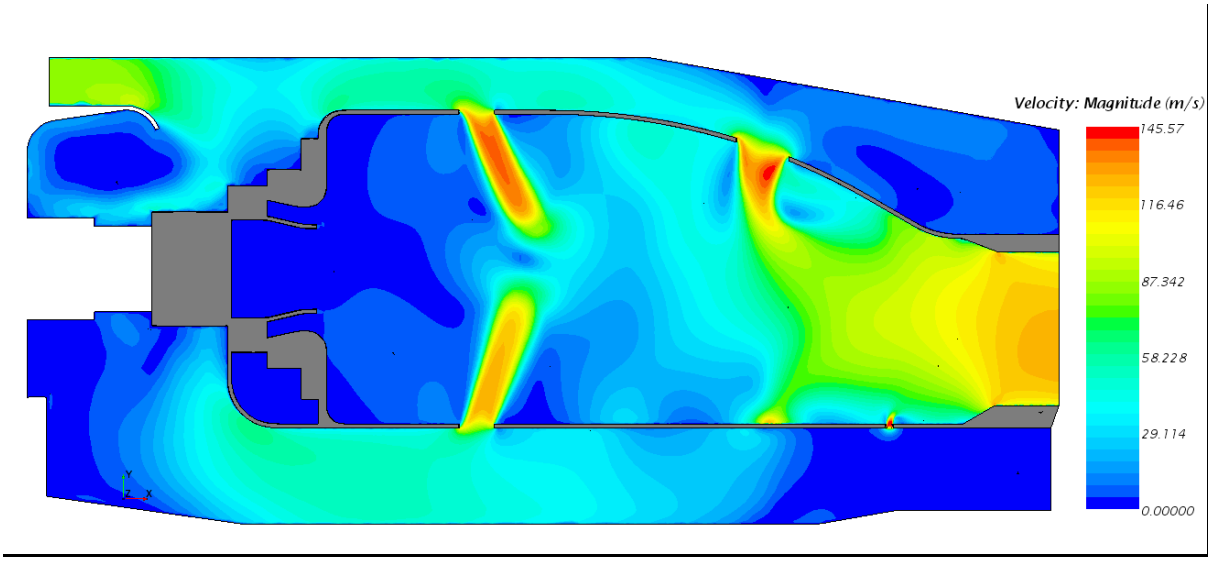

Figure 26: Velocity magnitude distribution on the main plane of mesh studies; 2400000.

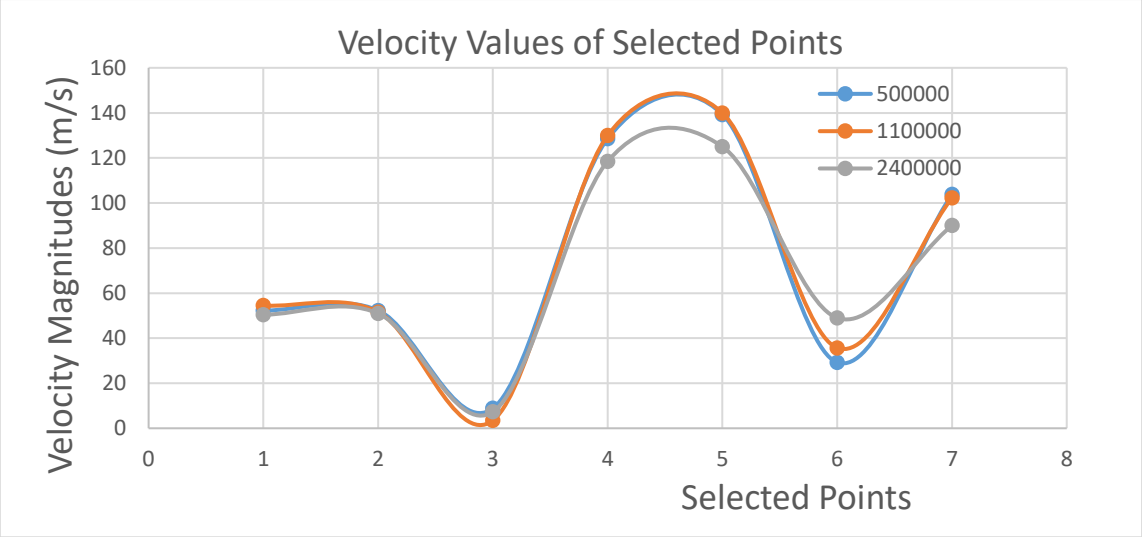

Figure 27: Velocity magnitudes of seven points inside of the geometry for different number of meshes; 500000, 1100000, 2400000.

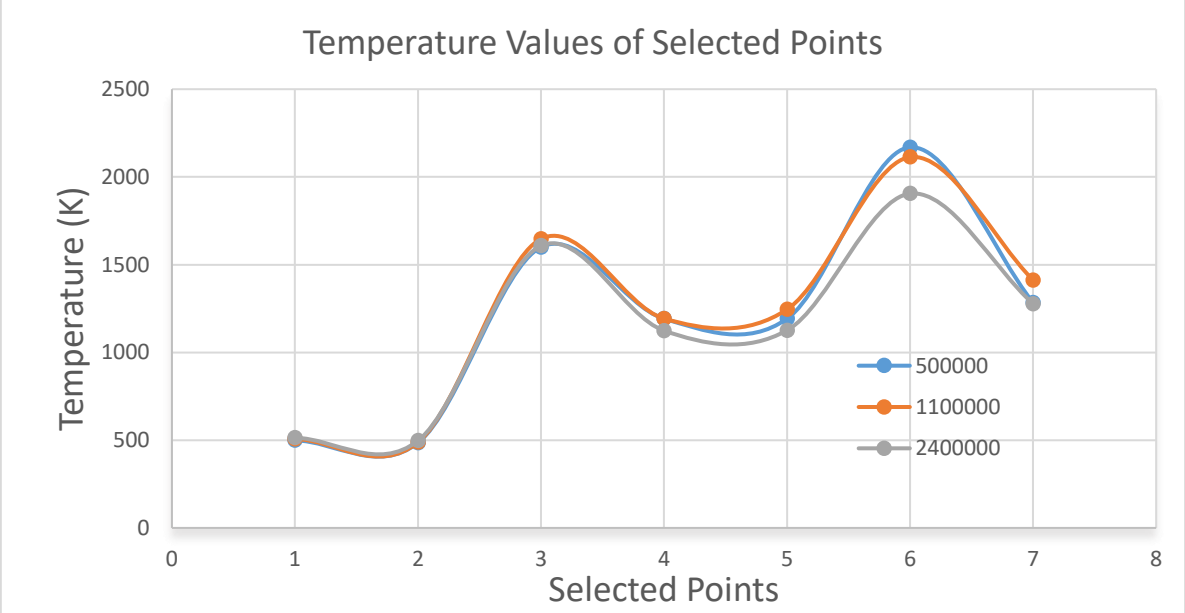

Figure 28: Temperature values of seven points inside of the geometry for different number of meshes; 500000, 1100000, 2400000.

When compared the temperature distribution on the main plane section, the first mesh gives overestimated results. The highest temperature on the main plane is around 2800 K whereas the second and the third have 2750 K as the highest temperature level. Moreover, the temperature distribution on the main plane of the second and the third one is so similar whereas the first one's temperature distribution is not.

In the figures 24, 25, and 26, the velocity distribution of these three different meshes can be compared. Like temperature distribution, the second and the third one's distribution are so similar, but the first mesh study is so different.

Finally several points inside of the geometry were selected, and their velocity magnitudes and temperature values were compared. The figures 27 and 28 shows these points' values. Overall, both the temperature and velocity distribution on the main plane section, and the velocity magnitudes and the temperature values show that the geometry with 1100000 gives reasonable results with companion of 2400000 meshes. In the simulations, the number of mesh has been determined as 1100000. It is also good in terms of solution time, this means half of the solution time is required when compared to 2400000 meshes, approximately.

4.2 The effect of gas properties

In first simulations, gas properties were used constant, but most properties of gases are dependent on temperature, so the flow, the combustion, and also heat transfer are really affected by selecting gas properties as constant or temperature-dependent. In the first simulations, n-dodecane was taken as a surrogate fuel. In order to see gas properties effect on the flow, two simulations' results will be compared. The scalar velocity and temperature distribution on the main plane will be compared. Both the simulations, Standard EBU model was used with the same mesh structure, that is, only gas properties were changed to see its effect on the simulation.

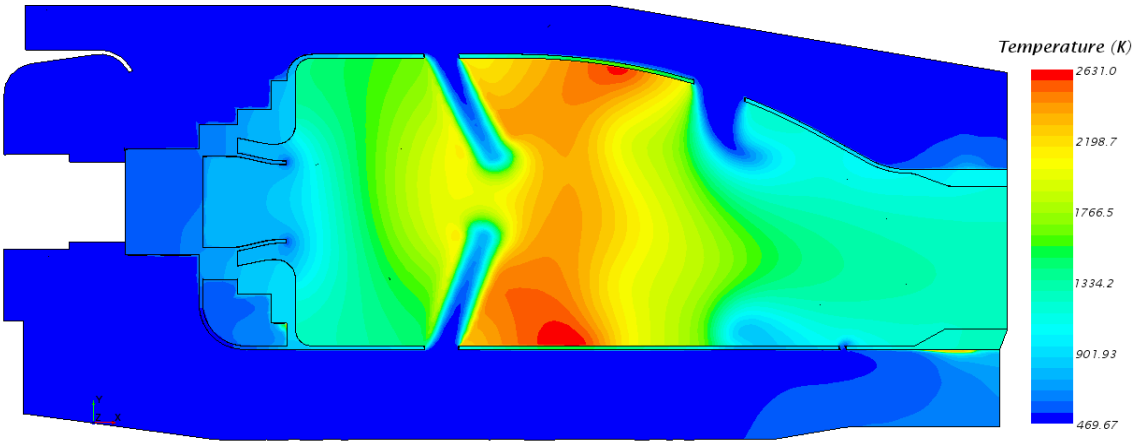

Figure 29: The temperature distribution on the main plane; gas properties are constant

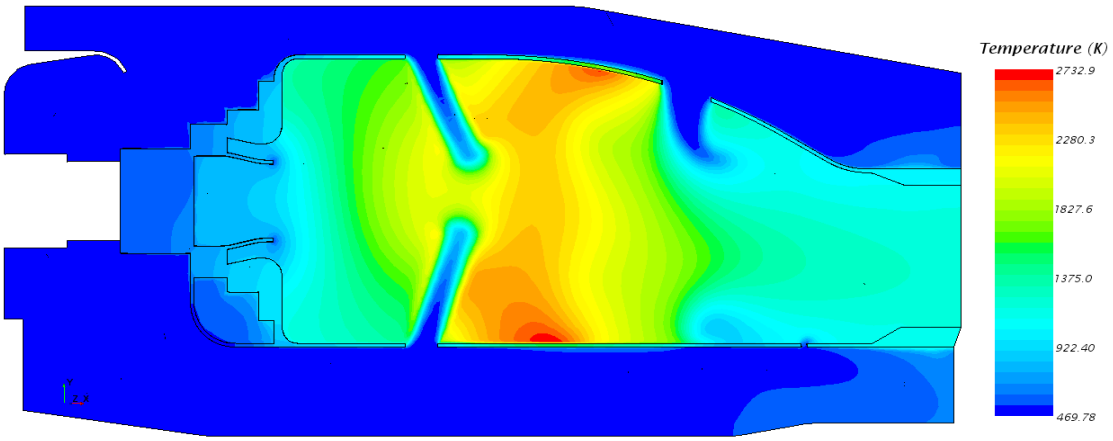

Figure 30: The temperature distribution on the main plane; gas properties are temperature-dependent

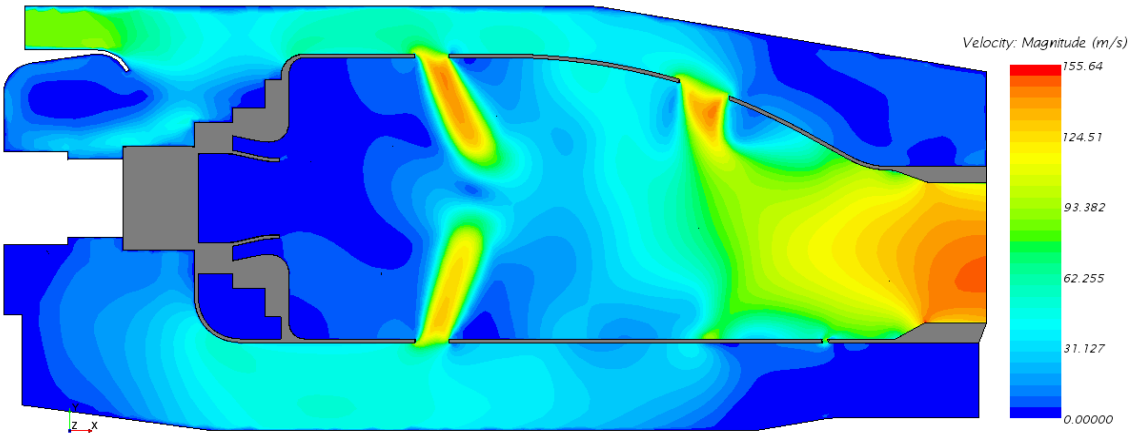

Figure 31: The velocity distribution on the main plane; gas properties are constant

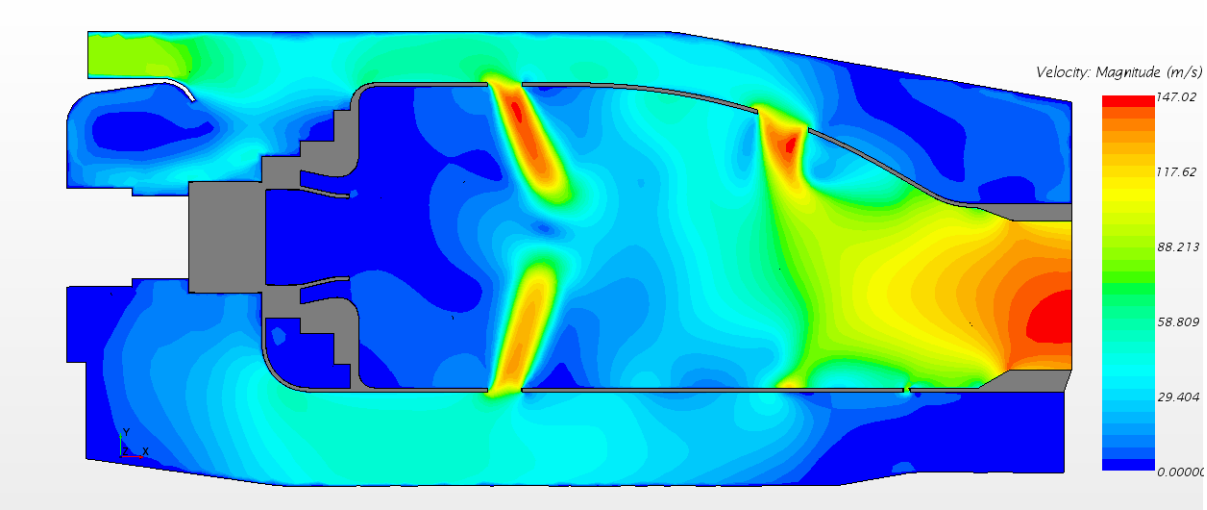

Figure 32: The velocity distribution on the main plane; gas properties are temperature-dependent

When compared to these two configurations, the general distribution of velocity on the main planes have similar to each other. The magnitudes of the velocities are affected approximately 7%, this also could affect liner wall temperature.

The gas properties do really affect temperature magnitudes, the highest temperature magnitudes are compared to each other, and to use gas properties as temperature-dependent affected the highest temperature approximately 100 K, this difference is going to have an effect on the liner wall temperature. So in combustion simulations, it is necessary to use gas properties as temperature-dependent because of having high-level temperatures inside of the flame tube.

4.3 The Effect of Using Fuel as Gas or Liquid

By assuming dynamic viscosity and some other properties as if gas, the fuel was used in gas phase by using the same number of meshes, the same combustion model, and so on.

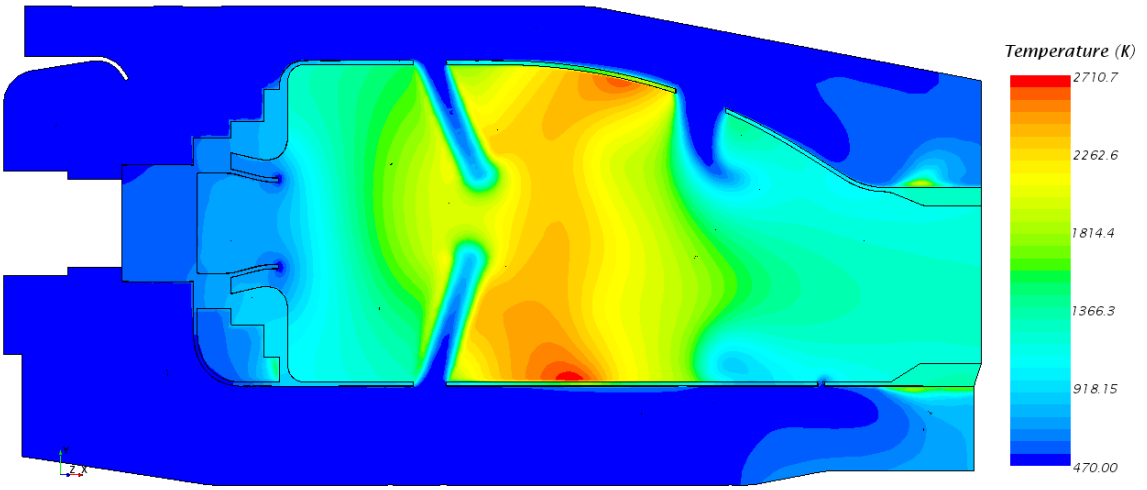

Figure 33: The temperature distribution on the main plane; the fuel was used in gas phase

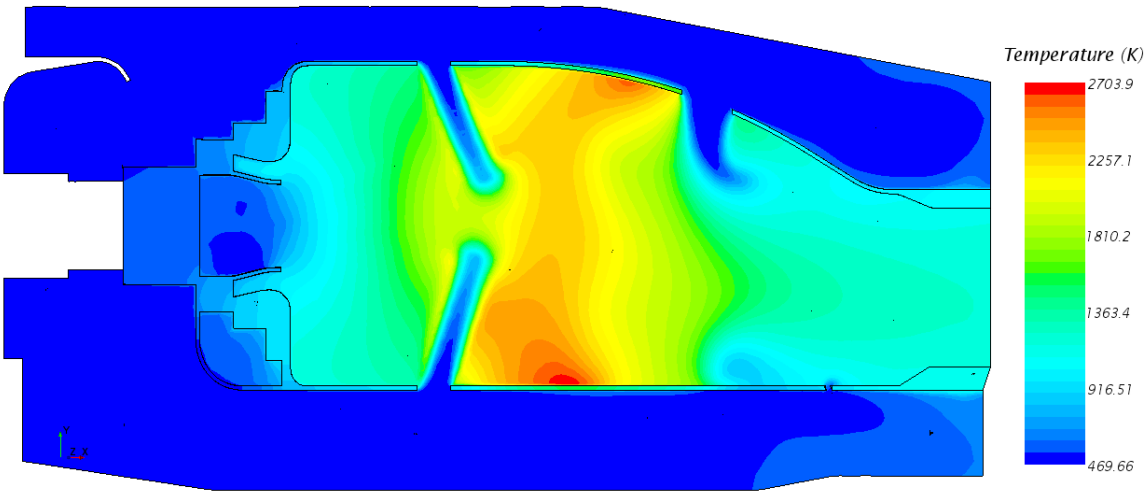

Figure 34: The temperature distribution on the main plane; the fuel was used in liquid phase

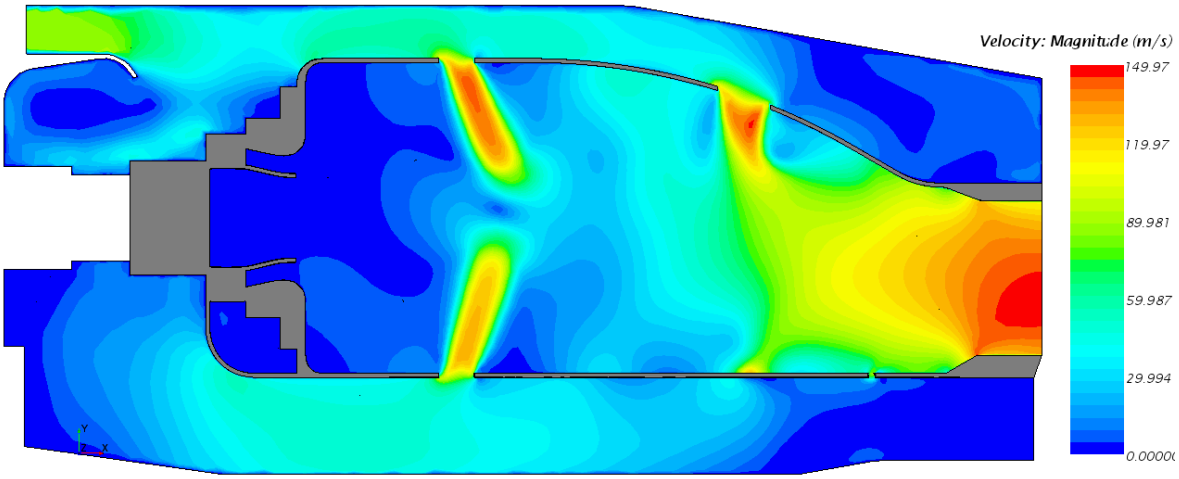

Figure 35: The velocity distribution on the main plane; the fuel was used in gas phase

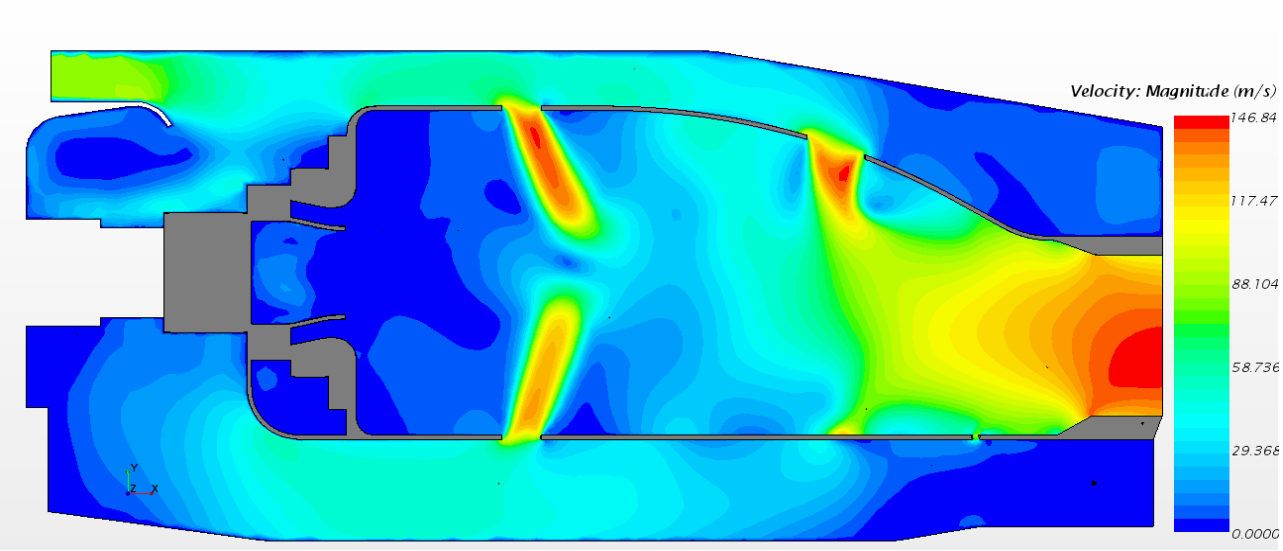

Figure 36: The velocity distribution on the main plane; the fuel was used in liquid phase

When compared both the temperature and the velocity distribution on the main plane section, both models have similar results. Additionally, the surface average of the two models were compared to each other. Gas phase model has an average outlet temperature around 1250 K, whereas when the fuel was defined as liquid, the average outlet temperature is around 1210 K as expected preliminary design. The difference results from the energy required for evaporation. Because of not using evaporation energy, the first model has high level temperature average in the outlet, this also caused to see high velocity

magnitudes at outlet. In order to obtain results from simulations, the liquid phase has to be used.

4.4 The Effect of Using Different Combustion Models

There are different types of combustion models in order to correspond the real combustion process. In this study two models were used; Standard Eddy Break up (EBU) and Presumed Probability Density Function (PPDF).

The main difference between these two combustion approaches is the reactions. In Standard EBU model, reactions and their properties are defined, then the simulation is run. In PPDF model, reaction are not defined, the main and intermediate species are defined, and PPDF equilibrium table is generated. It is estimated that in a real combustion of any hydrocarbon, there are more than 100 reactions and hundreds of intermediate species. To use more reactions in Standard EBU makes the results more realistic, but more solution time is required. Some of the applications use single-step, two-step, or four-step reduced mechanisms. To define around 50 reactions makes the solution time as much as two times more.

The comparison of these two combustion models were simulated for test case done by Topal. [37] The test case boundary conditions and the highest level of temperature measured on the liner wall are given below, and the simulations were done by using these parameters.

Table 4: Boundary conditions of the test case [37]

Inlet temperature	T_3	407.7 K
Outlet temperature	T_4	1101.2 K
Mass flow rate of the air	$\dot{m_{air}}$	0.1845 kg/s
Mass flow rate of the fuel	$\dot{m_{fuel}}$	0.00381 kg/s
Air-fuel ratio	AFR	48.4
Maximum wall temperature	T_{wall}	1123 K

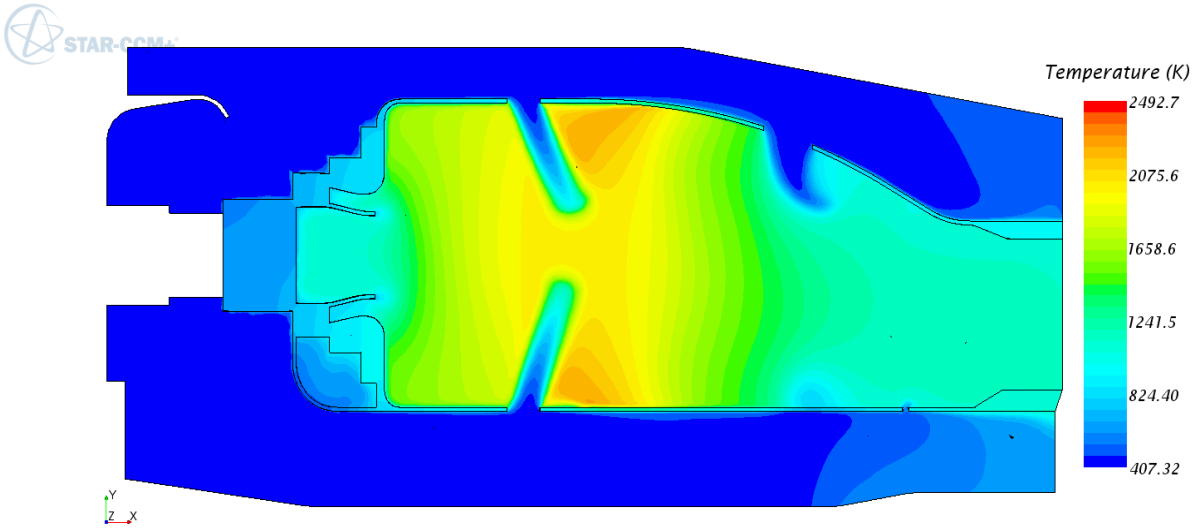

Figure 37: Temperature distribution on the main plane with the Standard EBU combustion model

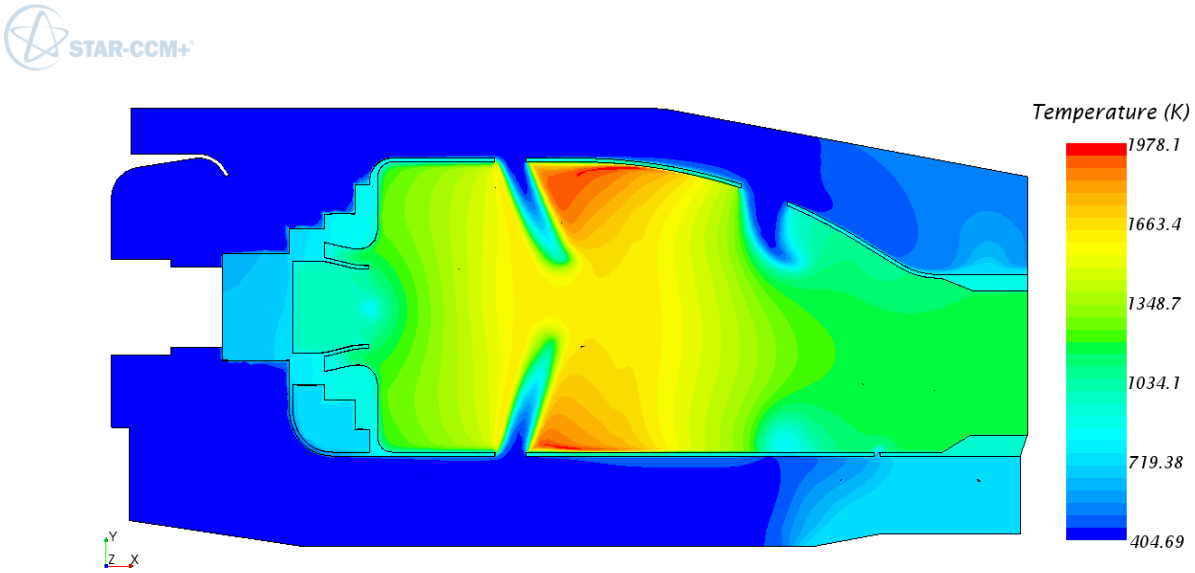

Figure 38: Temperature distribution on the main plane with the PPDF combustion model

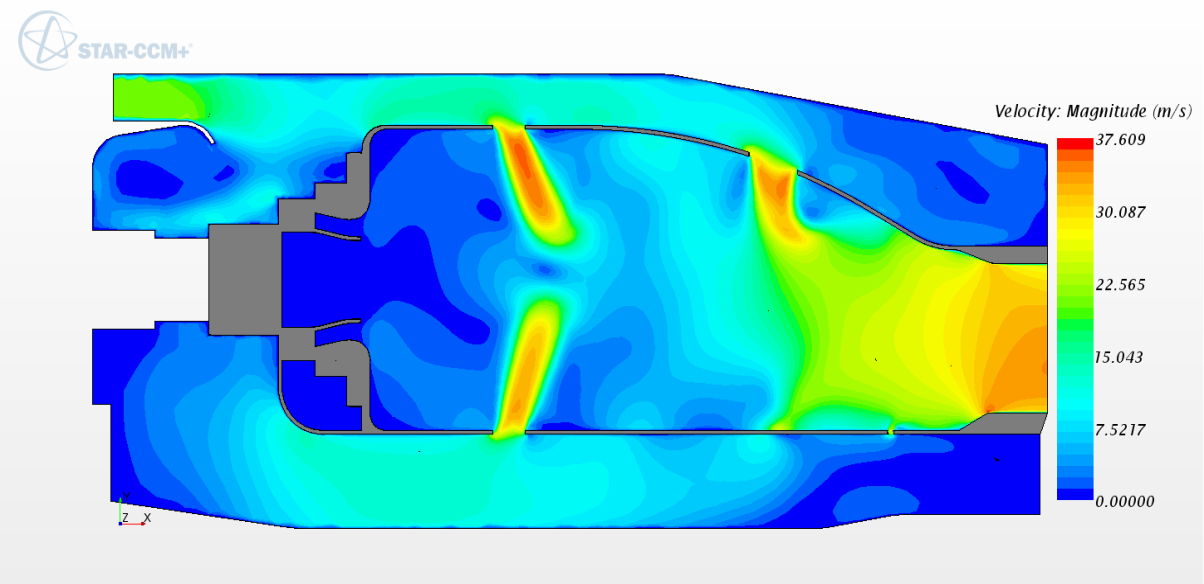

Figure 39: Scalar velocity distribution on the main plane with the Standard EBU combustion model

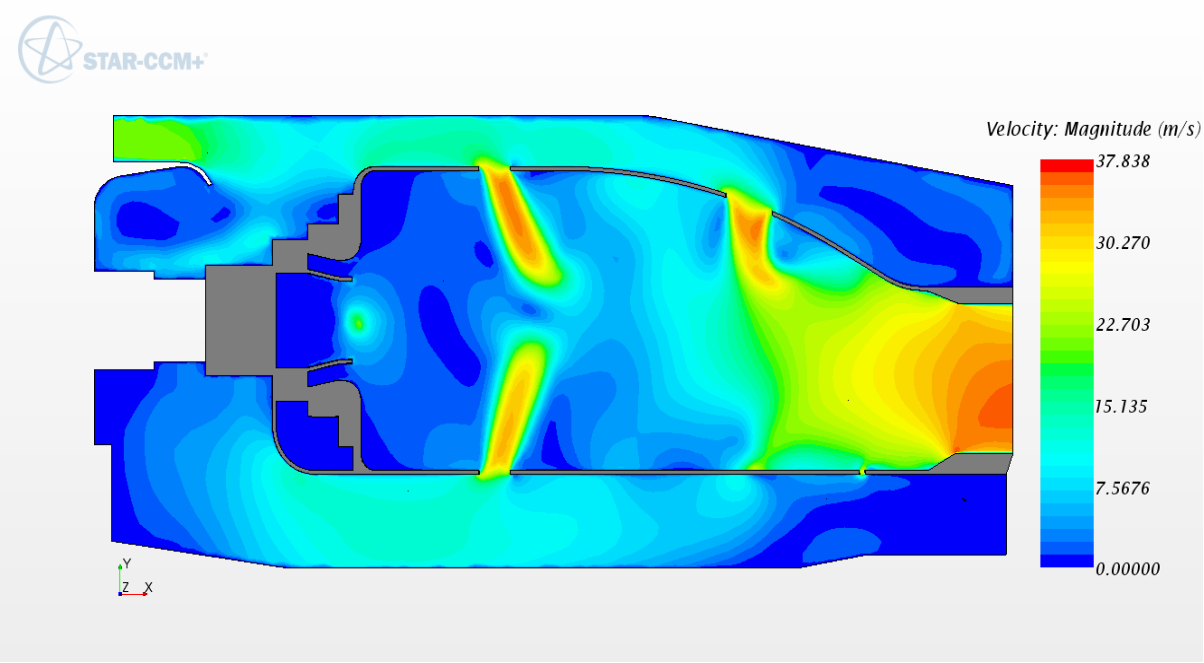

Figure 40: Scalar velocity distribution on the main plane with the PPDF combustion model

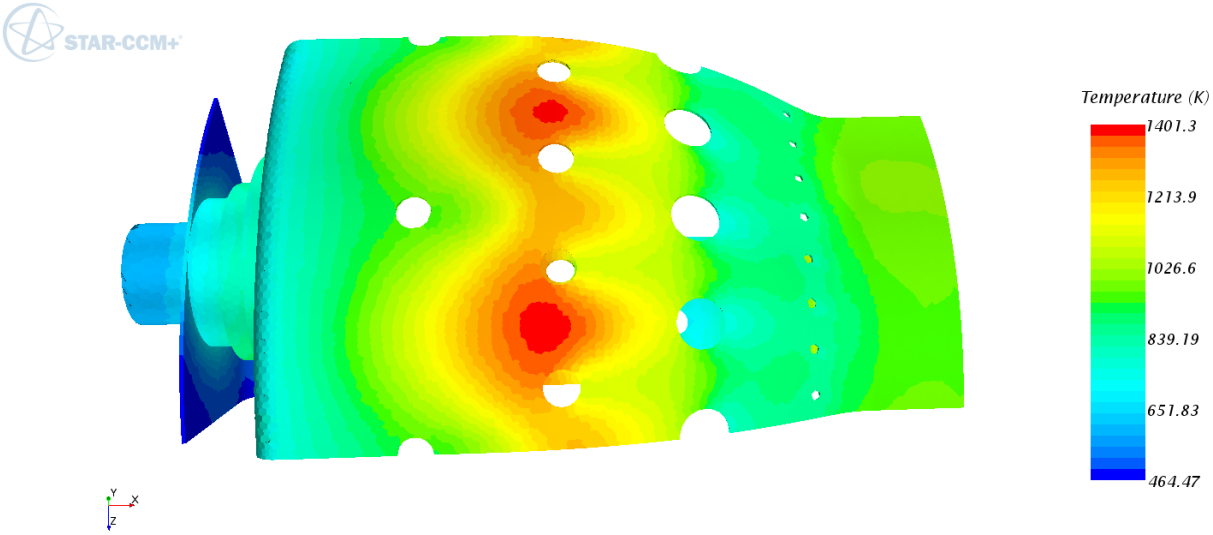

Figure 41: Temperature distribution on the liner wall with the Standard EBU combustion model

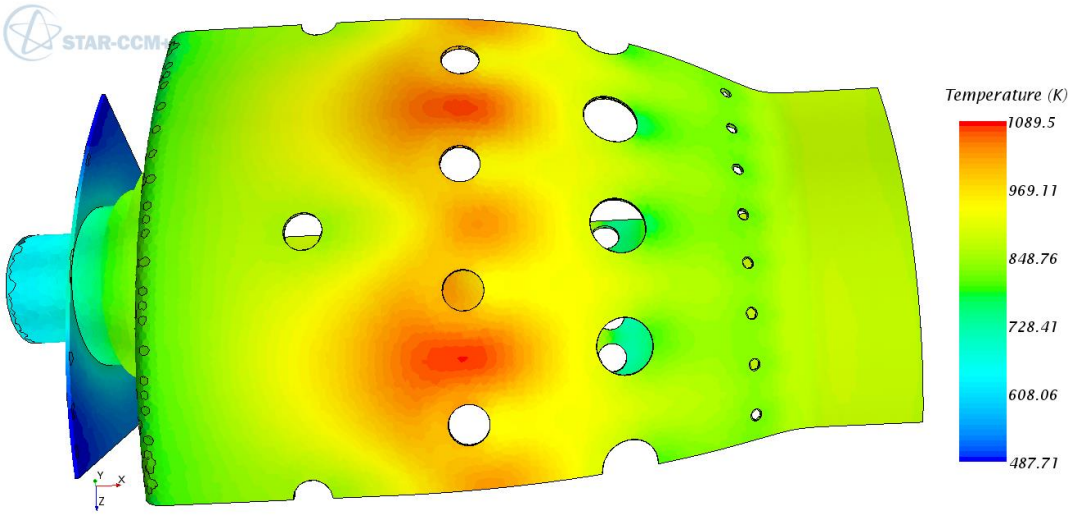

Figure 42: Temperature distribution on the liner wall with the PPDF combustion model

The comparison below was done by Star CCM+ and was reported, the comparison is about temperature-position estimations of PPDF and Standard EBU models. [68] As compared to test case and these two models, and the figure 43 show that Standard EBU model hasn't produced realistic results. PPDF model provides much more realistic results, so in next simulations, just PPDF Equilibrium combustion model will be used.

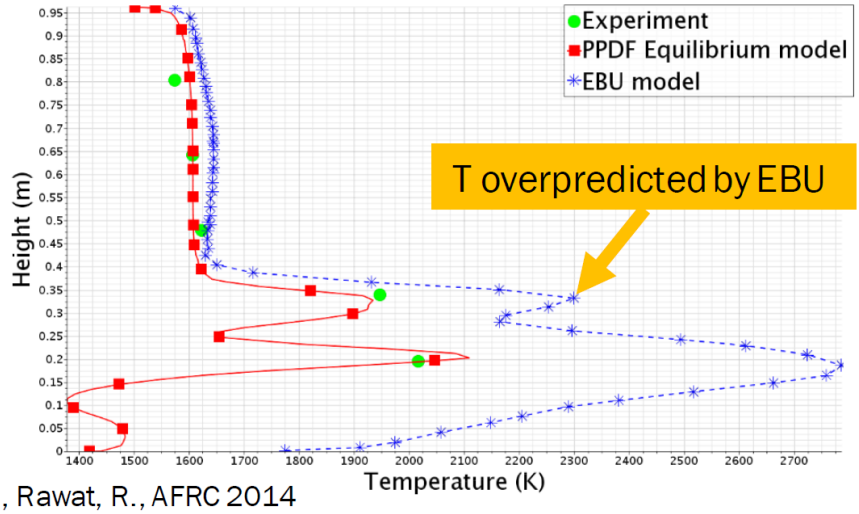

*Mallouppas, G., Zhang, Y., Rawat, R., AFRC 2014

Figure 43: A comparison of PPDF, Standard EBU models to experiment. [68]

4.5 The Effect of Using Different Number of Thin Meshes in Solid

The partition of the solid body is possible with the usage of thin meshing property. It is suggested that at least, 3 thin layer meshes should be used while simulating a conjugate heat transfer case. [57] In the simulations, 3 and 4 thin meshes were used in the solid domain with no change in the fluid domain. To use more thin meshes inside of the solid gives more accurate results. In this study, the effect of using different number of thin meshes will be examined, and the results will be compared with the experimental case by using PPDF combustion model and the other effects were cared.

The simulations were done by using boundary conditions, and given figures 44 and 45 shows that the more thin the meshes, the more accurate results have been obtained. In both simulations, 10 boundary layers were used with 2.1 mm total boundary layer thickness by considering that the first grid thickness is suitable for good y+ values.

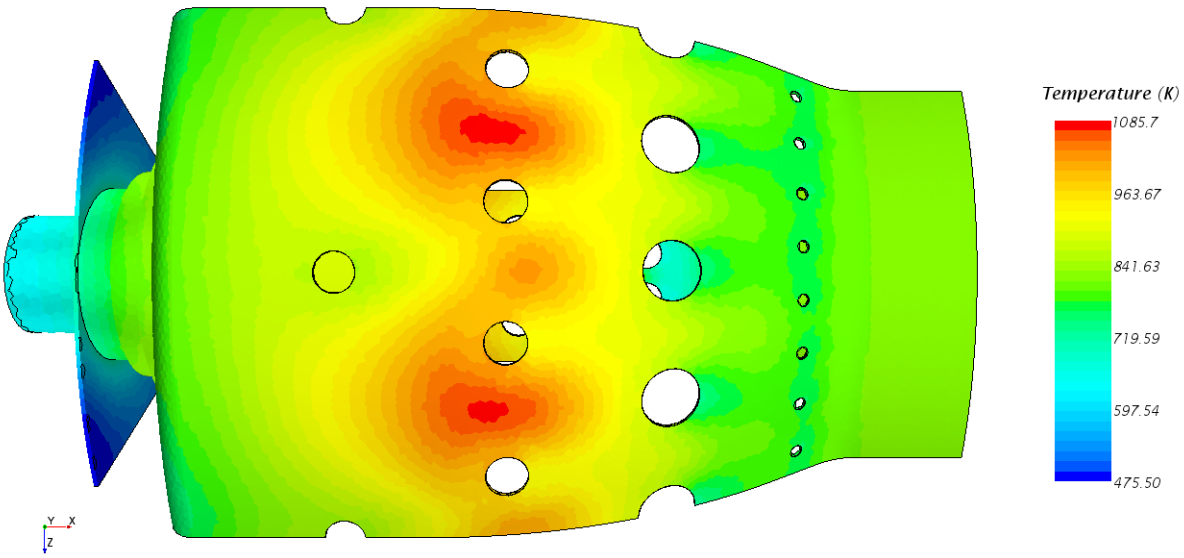

Figure 44: Wall temperature distribution with 3 thin meshes

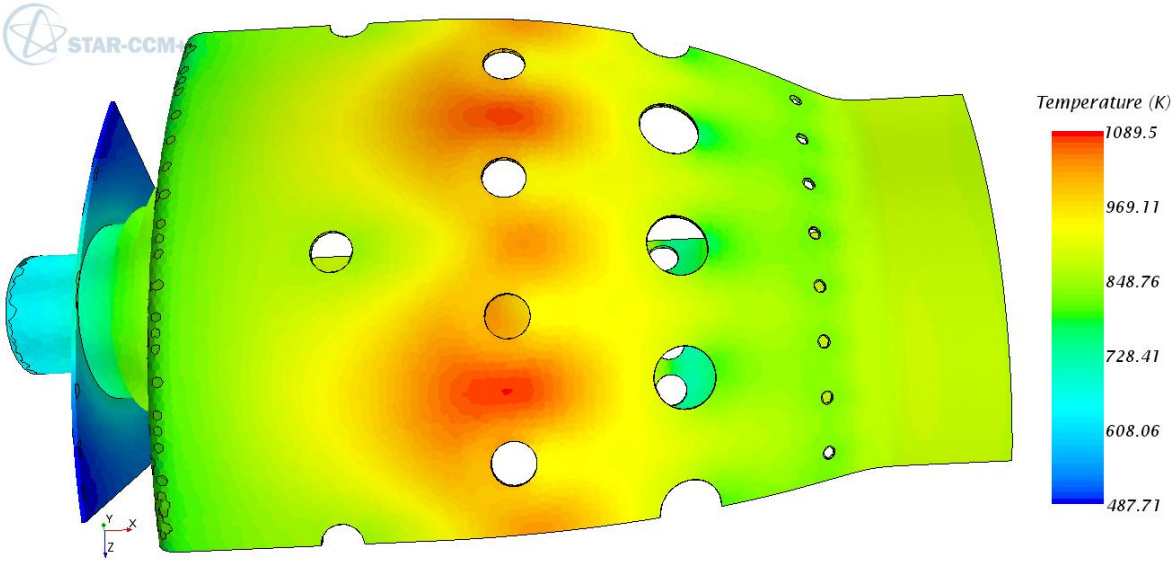

Figure 45: Wall temperature distribution with 4 thin meshes

When compared to experimental results, there is just 33 K difference in wall temperature. The most important reason for the difference is radiation effects on the liner wall temperature.

4.6 The Effect of Using Different Number of Boundary Layers with the Same Thickness

The simulations were done by using different number of boundary layers with the same thickness by the same first grid thickness. It is suggested that in order to have compatible conjugate heat transfer results with the experimental results, at least 10 boundary layers should be used. [57] In the simulations, 5, 10, 15, and 20 boundary layers with the same total thickness were used and compared.

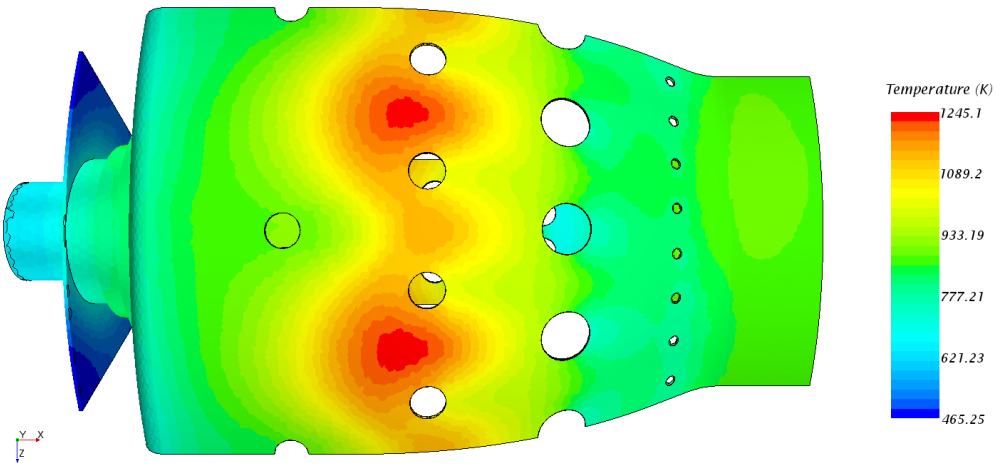

Figure 46: Wall temperature distribution with 5 boundary layers by saving first grid size

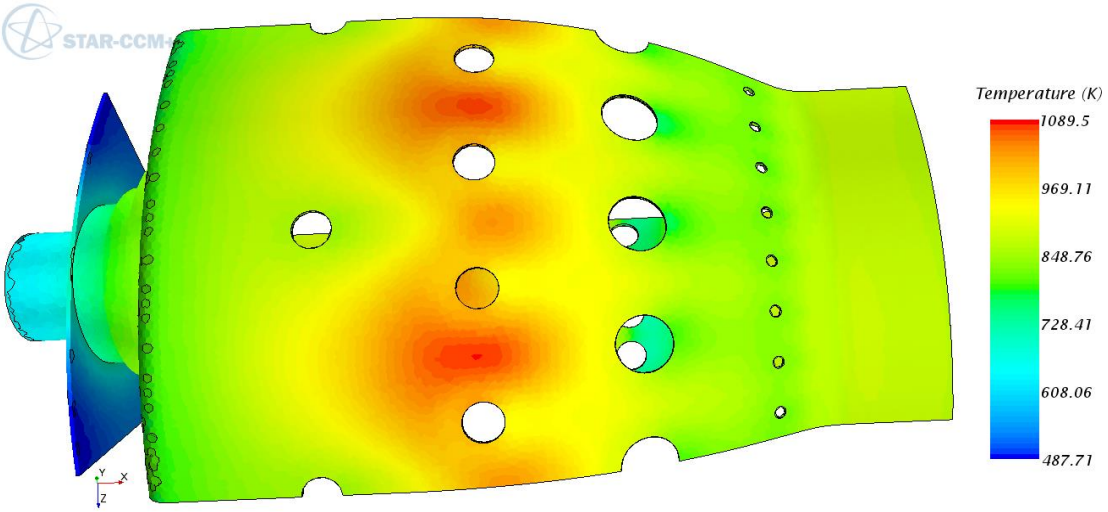

Figure 47: Wall temperature distribution with 10 boundary layers by saving first grid size

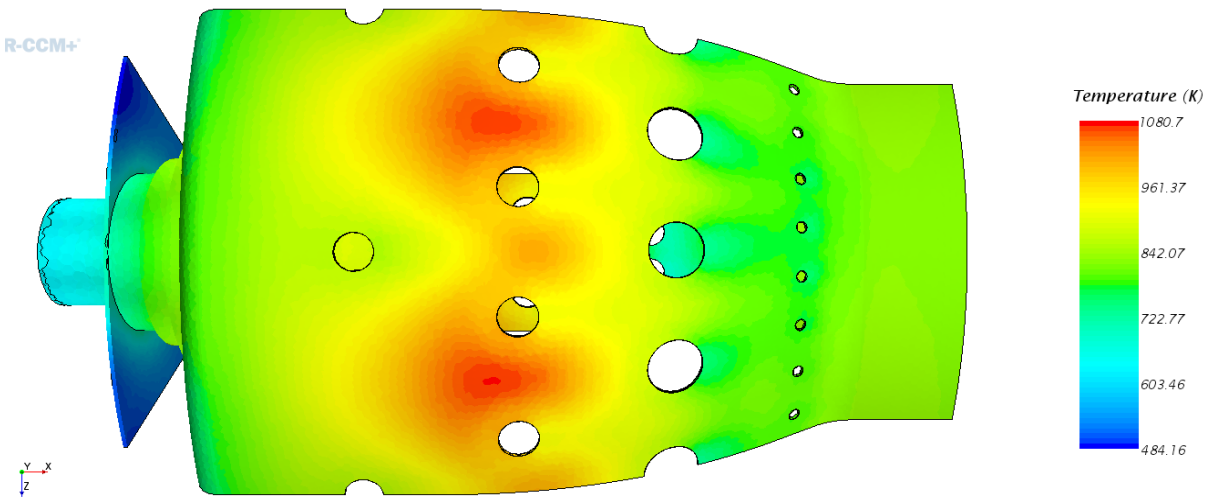

Figure 48: Wall temperature distribution with 15 boundary layers by saving first grid size

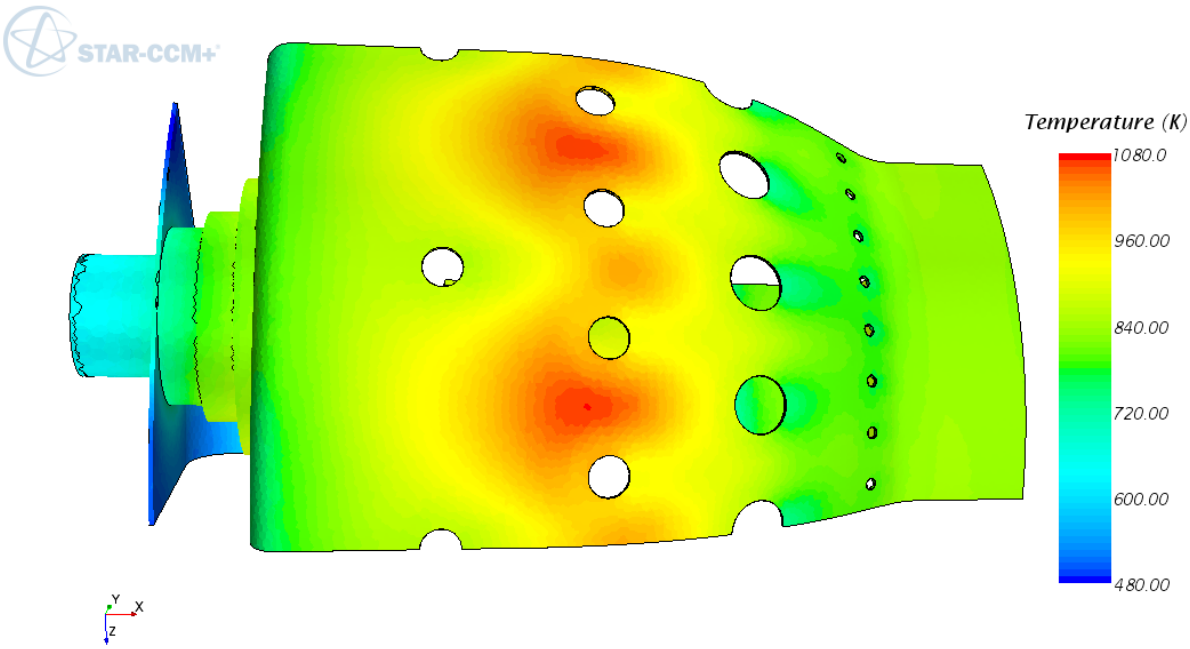

Figure 49: Wall temperature distribution with 20 boundary layers by saving first grid size

When compared these simulations' results especially liner wall temperature distribution on the liner wall, similar results have been obtained. As seen in the figure 42, 5 boundary layer mesh simulation overestimated the highest wall temperature when compared to others and experiment. The simulations which use 10, 15, and 20 boundary layers with the same thickness have almost the

same highest temperatures and the temperature distribution on the wall as well as the main plane section. Because of having similar results, to use 10 boundary layers is enough to reach reasonable results.

4.7 The Effect of Using Different Total Thickness of Boundary Layers with the Same Number of Boundary Layers

The previous part showed that approximately there is no difference among to use 10, 15, or 15 boundary layers. In this part, the effect of total thickness of the boundary layer will be examined by using 10 boundary layers. The simulations' results show that 10 boundary layer gave reasonable results when compared to test case. Different stretching ratios and different total thicknesses were used. The first grid size determination is so important, the main difference comes from the first grid size. Because in figure 50, the first grid size was 0.065 mm; in figure 51, it is 0.35 mm; in figure 52, it is 0.08 mm; and in figure 53, it is 0.09523 mm. The first grid size determines y+ values, and also the heat transfer from the gas to the solid.

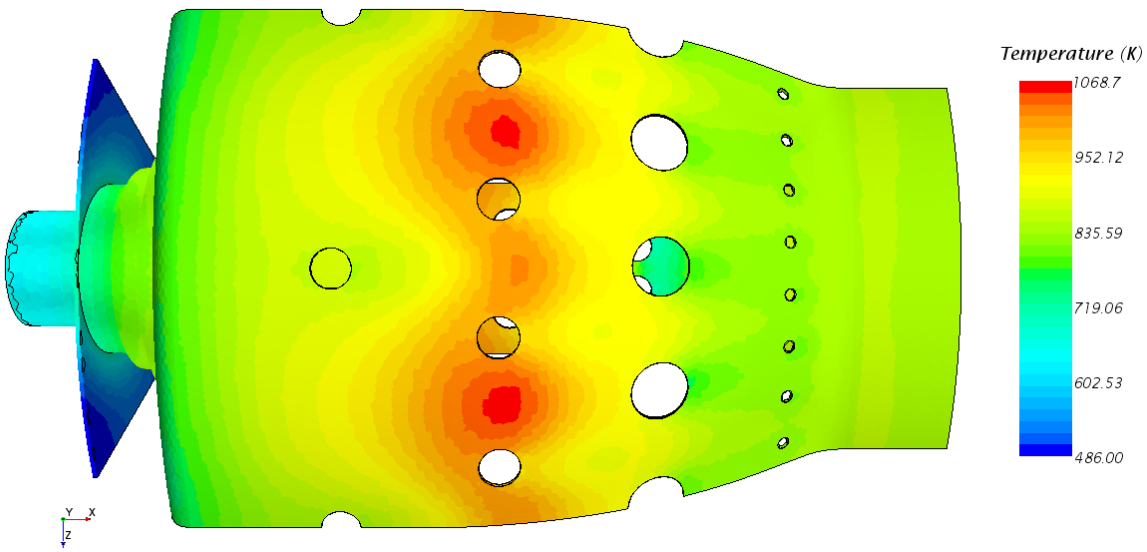

Figure 50: Temperature distribution on the liner wall with 0.65 mm boundary layer thickness, stretching ratio=1

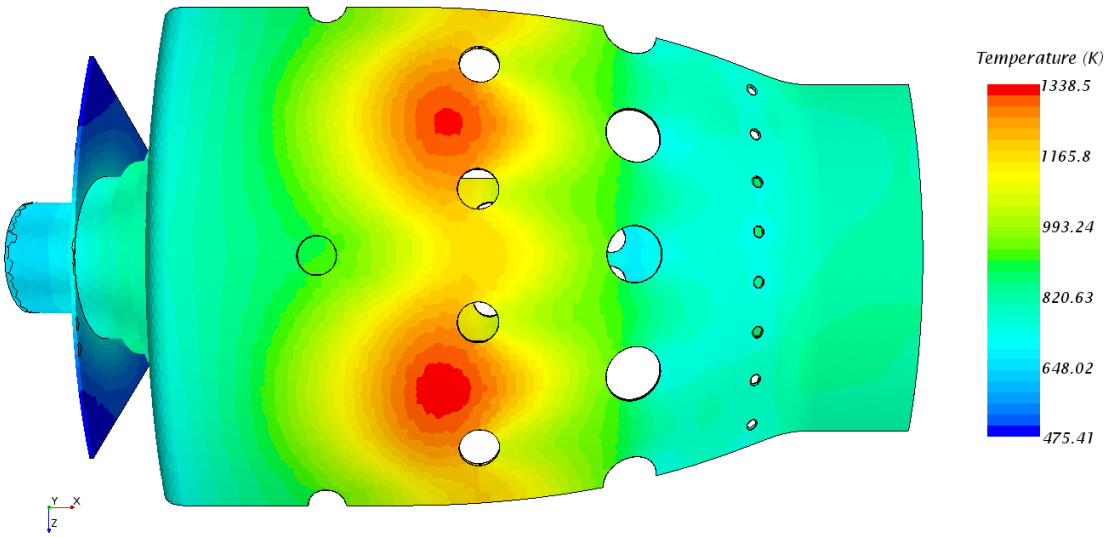

Figure 51: Temperature distribution on the liner wall with 3.5 mm boundary layer thickness, stretching ratio=1

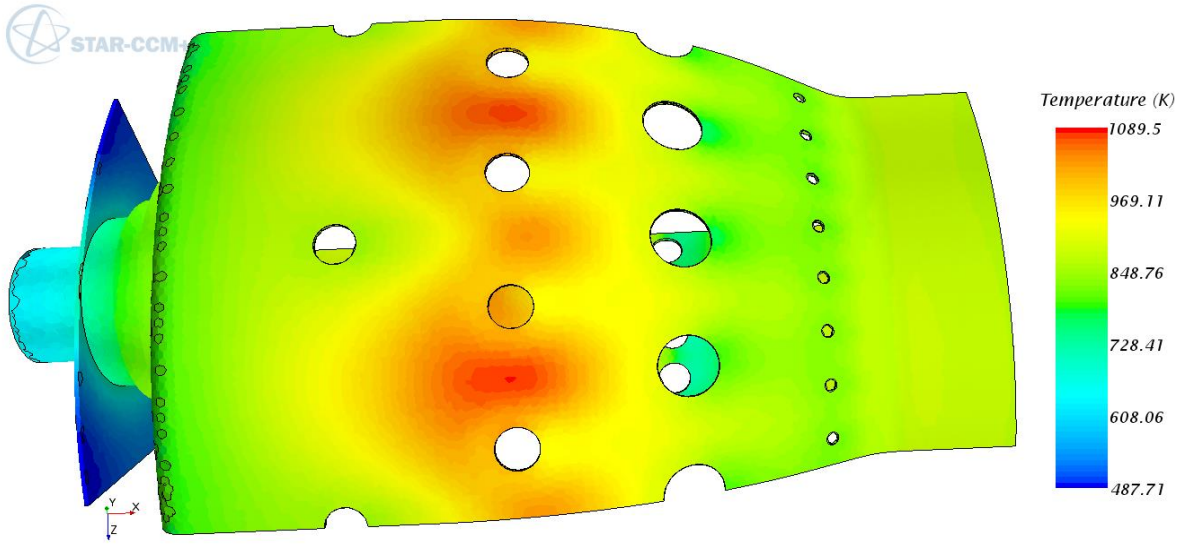

Figure 52: Temperature distribution on the liner wall with 2.1 mm boundary layer thickness, stretching ratio=1.2

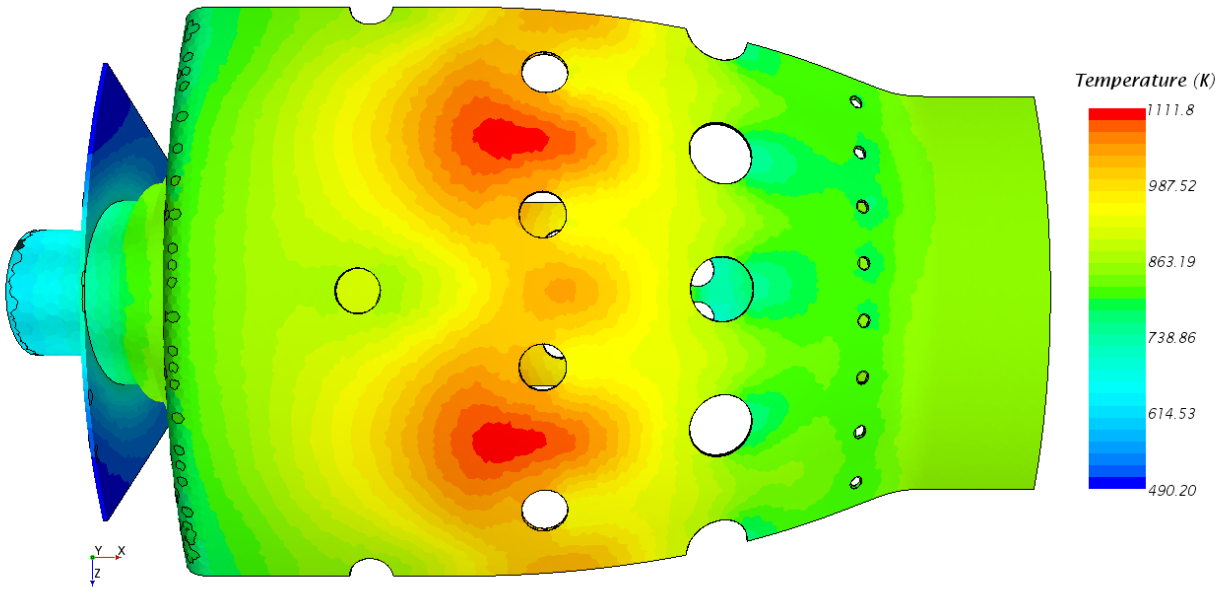

Figure 53: Temperature distribution on the liner wall with 2.5 mm boundary layer thickness, stretching ratio=1.2

There is a small difference between the test case and the latest work because of not modelling the radiation. According to simulations, the best suitable results with the test case was seen in the latest work, so in order to compute the liner wall temperature distribution on take-off conditions, 10 boundary layers will be used with 1.2 stretching and 2.5 mm total thickness.

4.8 Simulating the Geometry by Applying Take-off Boundary Conditions

A number of studies have been completed, by using different models and different methods, a lot of simulations have been done in order to obtain velocity, temperature distributions on the main plane, and liner wall temperature. As a result, the results obtained from the simulations were compared to experimental results. The best suitable simulation parameters like boundary layer thickness and the number of boundary layers were applied to one-seventh of the geometry, and the results are given below.

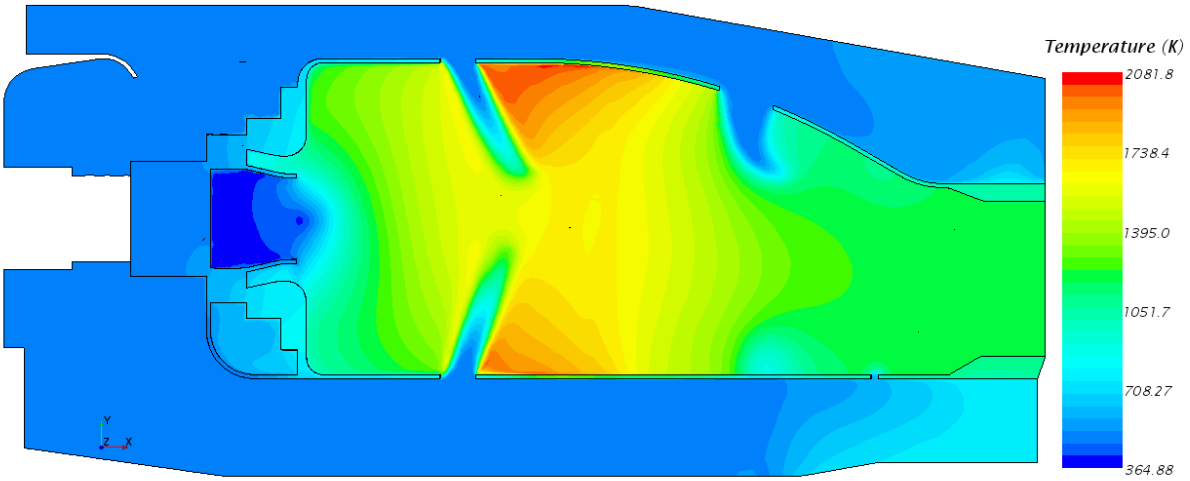

Figure 54: Temperature distribution on the main plane with the PPDF combustion model on take-off conditions

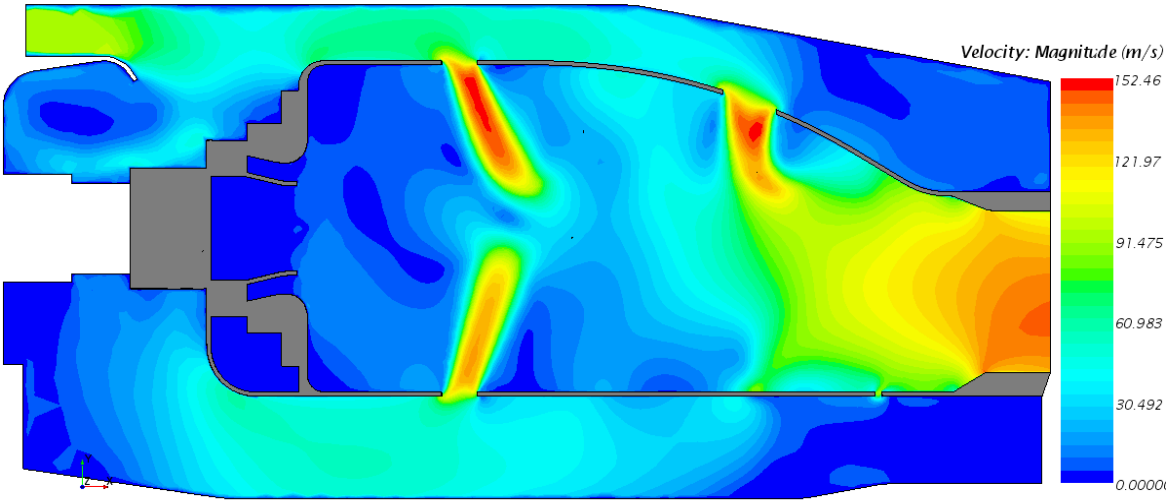

Figure 55: Scalar velocity distribution on the main plane with the PPDF combustion model on take-off conditions

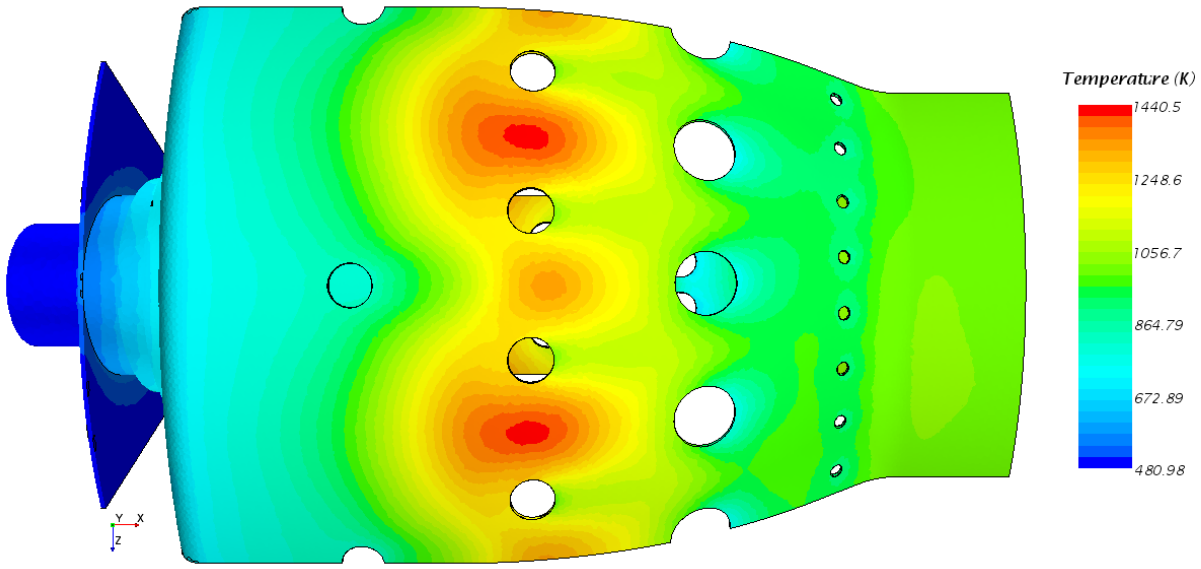

Figure 56: Temperature distribution on the liner wall on take-off conditions; with 2.5 mm boundary layer thickness, stretching ratio=1.2

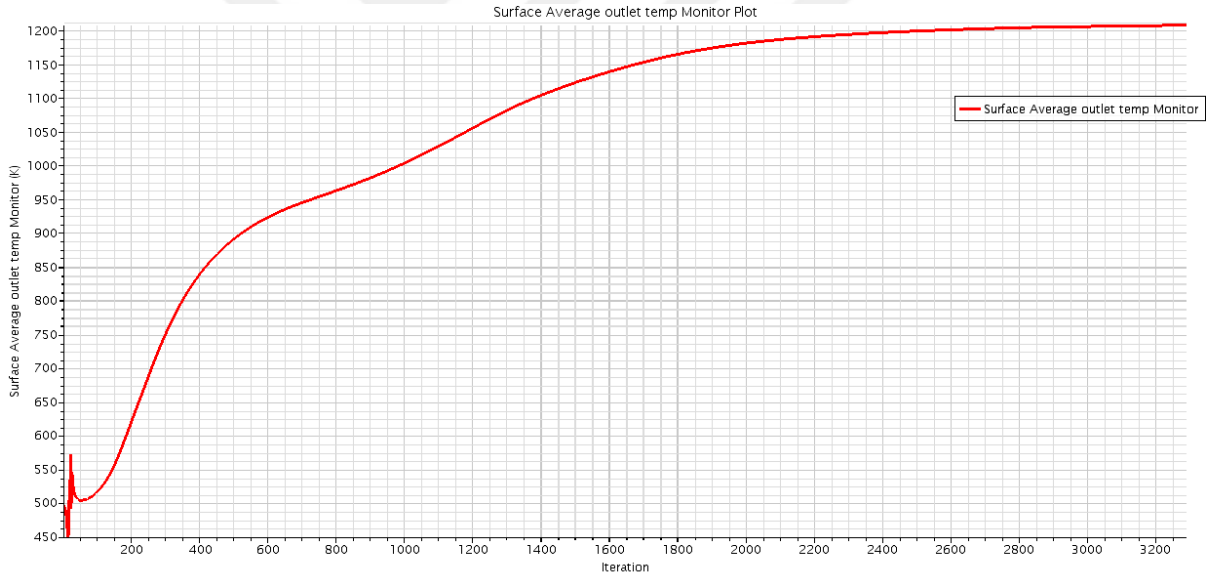

Figure 57: Surface average outlet temperature

As a result of test case simulations, the most compatible conjugate heat transfer parameters were applied to take-off conditions. Surface average outlet temperature was found as 1210 K as seen in the figure 57. 1200 K was aimed in the preliminary design with 96 % efficiency, CFD analysis show that the combustion efficiency is around 97.2 %. The liner wall temperature was computed as 1440 K, according to figure 56. When considering radiation effect,

it can jump to 1460-1470 K, but to model radiation costs too much, but it was thought as future work. The highest temperature on the main plane is around 2081 K, but in whole geometry, it is 2120 K. the highest flame temperature was calculated as 2200 K, the difference is coming from lower turbulent Prandtl and Schmidt number, and they were used as 0.25 in order to obtain suitable wall temperature distribution. Furthermore, liner wall temperature experiments must be done to compare with CFD.

5. CONCLUSION AND FURTHER WORK

In this study, after giving main components of a usual turbojet engine, the combustion chamber component was explained deeply. In literature survey, the importance of simulation, simulation parameters obtained from experiments, the importance of wall temperature and cooling, suggested combustion and turbulence models were explained. Because of modelling vorticities and swirls, realizable k-ε model was selected as a turbulence model. The spray parameters were considered regarding the combustion chamber pressure and injection pressure. Different combustion models were examined and compared to experimental values. Standard EBU and PPDF combustion models were decided to compare. Turbulent Prandtl and Schmidth numbers were critical to estimate wall temperature, and these two values were decided to be 0.25 for each. To simulate whole flow is too difficult, a number of solution models were compared. It was stated that Direct Numerical Simulation is just applicable for small Reynolds number (less than 10000), the Large Eddy Simulation is under progression but solution time is too much as well as expensive. Additionally, Detached Eddy Simulation (DES) method was developed to simulate inside of the flow by using LES method, and near wall treatment by using RANS. Because of being too much expensive and solution time, RANS model was decided to be used in the simulations.

In second part, combustion chamber design criteria and conceptual design parameters were introduced, and calculated for the geometry. Additionally, adiabatic flame temperature calculations and conjugate heat transfer process were calculated for the design.

In third part, mathematical modelling of gas and liquid phase were introduced. Conservation of mass, momentum and any scalar were defined. Moreover, the governing equations for fluids, Navier-Stokes equations in Cartesian coordinates, were given. The requirement for turbulence models was mentioned, additionally the turbulence models were introduced. Furthermore, the combustion models were introduced by giving important formulas for them.

In fourth part, Computational Fluid Dynamics (CFD) results were given. A number of simulations have been done, and the results were compared to each other or experimental values. Firstly, a mesh study was done by using approximately 500000, 1100000, and 2400000 polyhedral meshes. The results were compared to each other, and to use 1100000 polyhedral containing mesh work is suitable for the study, and this was used for later studies.

Second part of the CFD analysis was about the effect of using gas properties as constant or temperature-dependent. The analysis were done by changing only gas properties as constant and temperature-dependent. Simulations were done by using n-dodecane with real boundary conditions with the same mesh structure, the same combustion model, and so on. As a result of this study, combustion chamber analysis should be done by considering temperature-dependent gas properties because of high-level temperatures inside the flame tube.

Third part of the CFD analysis was about using the fuel as gas phase or liquid phase. As a result of this study, usage of fuel as gas or liquid phase didn’t affect the temperature and velocity distributions on the main plane but at the outlet,

surface average temperature of gas phase simulation was higher than the other because of evaporation energy.

Fourth part of the CFD analysis was about the combustion models used in the analysis. It is also stated by Star CCM+, Standard EBU model overestimates the temperature while PPDF model has compatible results with experiment. In this part, the PPDF combustion model was decided to use in the simulations. In this part of the study, test case conditions were used and compared to experimental results.

Fifth part of the CFD analysis was about the effect of using different number of thin meshes in the solid domain. In this part, by applying test conditions, test case were simulated by using 3 and 4 thin meshes in the solid domain. As a result, there is no significant difference between these two conditions but to use 4 thin meshes provides more precise values. In later studies, 4 thin meshes will be used.

Sixth part of the CFD analysis was about the effect of using different number of boundary layers by protecting total thickness and the first grid size near wall. The results were compared, and there was no significant difference between usages of 10, 15, and 20 boundary layers. However, to use 5 boundary layers overestimated. In later works, 10 boundary layers will be used.

Seventh part of the CFD analysis was about the total thickness of boundary layers. The number of boundary layers were 10 as suggested previous part.

Eight part of the CFD analysis was simulation of the geometry by applying take-off boundary conditions.

In this study, a number simulations were done in order to investigate liner wall temperature of a small turbojet engine. According to simulations and comparisons, these results have been obtained;

- Suitable number of meshes should be used,
- Gas properties should be used as temperature-dependent,
- The fuel should be used in liquid phase,
- PPDF combustion model should be used if the reactions aren't known exactly,
- At least 4 thin meshes should be used in the solid domain, to use more extends solution time, and to use less gives non-sensitive results,
- At least 10 boundary layers should be used by considering the first grid size,
- To use different boundary layer thickness with the same number of boundary layers affect the temperature distribution, it determines y+ and the heat transfer.

As a result the highest temperature of the liner wall was investigated as 1460 K with regarding radiation effect, while the melting point of the metal is more than 1550 K. The result is approximate because of non-modelling radiation. To be in the safe side, a number of suggestions will be provided in the future works.

Future Work

Radiation will be modelled in later works, because it is a significant part of the heat transfer from hot gas to the liner wall. Different combustion models might be used. With an acceptable number of meshes, Detached Eddy Simulation will be used in order to see near wall treatment and the flow better. Additionally, advanced layer mesh properties will be used to reduce approximation errors.

6. REFERENCES

[1] Rolls-Royce, the Jet Engine, *Rolls-Royce PLC*, Derby, 1996.

[2] Grant, R.G., Flight: *The Complete History*, DK Publishing, New York, 2007.

[3] *Father of the jet age* (1943) Available at: http://www.vulcantothesky.org/history/articles-of-interest/father-of-the-jet-age.html (Accessed: 24 August 2016).

[4] The Globe. 2015. *Throwback Thursday: Whittle and von Ohain fly first jet aircraft in 1939*. [ONLINE] Available at: http://globe.erau.edu/throwback-thursday-whittle-and-von-ohain-fly-first-jet-aircraft-in-1939/. [Accessed 12 August 2016].

[5] *Turbo jet* (2015) Available at: http://www.petervaldivia.com/turbo-jet/ (Accessed: 24 August 2016).

[6] *Brayton cycle* (2011) Available at: http://aviationknowledge.wikidot.com/aviation:brayton-cycle (Accessed: 24 August 2016).

[7] Cohen, H., Rogers, G.F.C., Saravanamuttoo, H.I.H. and Cohen, H. (1996) *Gas turbine theory*. 4th edition. Harlow, Essex: Longman Group.

[8] *How is fuel mixed with air in a jet engine?* (2016) Available at: http://engineering.stackexchange.com/questions/664/how-is-fuel-mixed-with-air-in-a-jet-engine (Accessed: 24 August 2016).

[9] Academic (2010) *Combustor*. Available at: http://en.academic.ru/dic.nsf/enwiki/617304 (Accessed: 24 August 2016).

[10] Peters, J. (2014) *Jet propulsion: Combustion chamber*. Available at: http://www.slideshare.net/jesscar/jet-engines-lesson-2 (Accessed: 22 August 2016).

[11] (2014) Available at: http://cset.mnsu.edu/engagethermo/documents/Combustion%20chamber.pdf (Accessed: 22 August 2016).

[12] Lawson, R. J., *Computational Modelling of an Aircraft Engine Combustor to Achieve Ta Temperature Profiles*, ASME Paper 93-GT-164, 1993.

[13] Lefebvre, A.H., *Gas Turbine Combustion*, Taylor & Francis, New York, 1999.

[14] Murthy, J.N., 1988, *Gas Turbine Combustor Modelling for Design*, Doctoral Research, Cranfield Institute of Technology, Mechanical Engineering, Cranfield.

[15] Walsh, P.P. and Fletcher, P., *Gas Turbine Performance*, Pennwell Books, Tulsa, 1998.

[16] Lefebvre, A.H. and Norster, E.R., *The Design of Tubular Combustion Chambers for Optimum Mixing Performance, Proceedings of the Institution of Mechanical Engineers*, 183, 150-155, 1969.

[17] Kaddah, K.S., 1964, *Discharge Coefficients and Jet Deflection Angles for Combustor Liner Air Entry Holes*, Master's dissertation, Cranfield Institute of Technology, Aeronautical Engineering, Cranfield.

[18] Freeman, B.C., 1965, *Discharge Coefficients of Combustion Chamber Dilution Holes*, Master's dissertation, Cranfield Institute of Technology, Aeronautical Engineering, Cranfield.

[19] Carotte, J.F. and Stevens, S.J., *The Influence of Dilution Hole Geometry on Jet Mixing*, Journal of Engineering for Gas Turbines and Power, 112, 73-79, 1990.

[20] Sauter, J., Die Grössenbestimmung der in Gemischnebeln von Verbrennungskraftmaschinen vorhandenen Brennstoffteilchen, VDI-Forschungsheft, 279, 1926.

[21] Mouldi Chrigui, Ilia V. Roisman, Feras Z. Batarseh, Amsini Sadiki, and Cam Tropea, Journal of Propulsion and Power 2010 26:6, 1170-1183

[22] Hamid A, Ahmad Hussein Abdul Hamid. *Spray cone angle and air core diameter of hollow cone swirl rocket injector.* IIUM engineering journal: 12/01/2011; 12(3).

[23] Santolaya, J. L., et al. (2010). *Analysis by droplet size classes of the liquid flow structure in a pressure swirl hollow cone spray*. Chemical Engineering and Processing: Process Intensification 49(1): 125-131.

[24] Little, A.R. and Manners, A.P., *Predictions of the Pressure Losses in 2D and 3D Model Pump Diffusers*, ASME Paper 93-GT-184, 1993.

[25] Srinivasan, R., Freeman, W.G., Mozumdar, S. and Grahman, J.W., *Measurements in an Annular Combustor-Diffuser System*, AIAA Paper 90-2162, 1990.

[26] Karki, K.C., Oeclsle, V.L. and Mongia, H.C., *A Computational Procedure for Diffuser-Combustor Flow Interaction Analysis*, Journal of Engineering for Gas Turbines and Power, 114, 1-7, 1992.

[27] Mongia, H.C, *Combustion Modeling in Design Process: Applications and Future Direction*, AIAA Paper 94-0466, 1994.

[28] Lai, M.K., *CFD Analysis of Liquid Spray Combustion in a Gas Turbine Combustor*, ASME Paper 97-GT-309, 1997.

[29] Crocker, D.S., Nickolaus, D. and Smith, C.E., *CFD Modeling of a Gas Turbine Combustor From Compressor Exit to Turbine Inlet*, Journal of Engineering for Gas Turbines and Power, 121, 89-95, 1999.

[30] Smiljanovski, V. and Brehm, N., *CFD Liquid Spray Combustion Analysis of a Single Annular Gas Turbine Combustor*, ASME Paper 99-GT-300, 1999.

[31] Malecki, R., Rhie, C., McKinney, R., Ouyang, H., Syed, S., Colket, M., and Madabhushi, R., *Application of an Advanced CFD-Based Analysis System to the PW6000 Combustor to Optimize Exit Temperature Distribution. Part I: Description and Validation of the Analysis Tool*, ASME Paper 2001-GT-0062, 2001.

[32] di Mare, F., Jones, W.P. and Menzies, K.R., *Large Eddy Simulation of a Model Gas Turbine Combustor, Combustion and Flame*, 137, 278–294, 2004.

[33] Boudier, G., Gicquel, L.Y.M., Poinsot, T., Bissieres, D. and Berat, C., *Comparison of LES, RANS and Experiments in an Aeronautical Gas Turbine Combustion Chamber*, Proceedings of the Combustion Institute, 31, 3075–3082, 2007.

[34] Nanduri, J.R., Parsons, D.R., Celik, I.B. and Strakey, P.A., *Analysis of the Emission Prediction Capabilities of RANS Based Turbulent Combustion Models for Lean Premixed Combustion of Methane*, International ANSYS Conference, Pittsburgh, USA, 2008.

[35] Brink, A., Mueller, C., Kilpinen, P. and Hupa, M., *Possibilities and Limitations of the Eddy Break Up Model*, Combustion and Flame, 129, 275-279, 2000.

[36] Celik, E., *Computational Fluid Dynamics Analysis Of Spray And Combustion Characteristics Of A Combustion Chamber With Prefilming Air-*

Blast Atomizer, Master's Dissertation, Tobb University of Economics and Technology, Mechanical Engineering, 2012.

[37] Topal, A., *Combustor Design, Test and Thermodynamic Analysis for A Small Scale Turbojet Engine*, Master of Science Thesis, Anadolu University, Department of Airframe and Powerplant Maintenance, 2014.

[38] Singh, S. N., Seshadri V., Singh R. K., Mishra T., *Flow Characteristics of an Annular Gas Turbine Combustor Model for Reacting Flows Using CFD*, Journal of Scientefic & Industrial Research, Vol. 65, 2006

[39] CFX Validation Report, *Heat transfer predictions using advanced two-equation turbulence models*, 2012.

[40] Westbrook, C.K., and Dryer, F.L., *Simplified Reaction Mechanisms for the Oxidation of Hydrocarbon Fuels in Flames*, Combustion Science and Technology, 27, 31-43, 1981.

[41] Mauss, F., Peters, N., *Reduced Kinetic Mechanisms for Premixed Methane-Air Flames*, Institut fur Technische Mechanik, Germany, 2008.

[42] Boudier, G., Gicquel, L.Y.M., Poinsot, T., Bissieres, D., Berat, C., LES *Predictions and Validations of the Exit Temperature Profiles in an Industrial Combustion Chamber*, CERFACS, IMFT, TURBOMECA, France,

[43] Gouws, J. J., *Combining a One-Dimensional Empirical and Network Solver with Computational Fluid Dynamics to Investigate Possible Modifications to a Commercial Gas Turbine Combustor*, University of Pretoria, Faculty of Mechanical/Aeronautical Engineering, 2007

[44] Odgers J., *Combustion Modelling within Gas Turbine Engines, Some Applications and Limitations*, AGARD CP 275

[45] INCONEL 625 alloy, *Physical Constants and Thermal Properties Report*, 2013.

[46] Tennekes, H. and Lumley, J.L., *A First Course in Turbulence*, The MIT Press, Boston, 1972.

[47] Richardson, L.F., *Weather Prediction by Numerical Process*, Cambridge University Press, Cambridge, 1922.

[48] Kolmogorov, A.N., *The Local Structure of Turbulence in Incompressible Viscous Fluid for Very Large Reynolds Numbers*, Doklady Akademii Nauk SSSR, 30, 299–303, 1941.

[49] Poinsot, T. and Veynante, D., *Theoretical and Numerical Combustion*, R.T. Edwards, Inc., Toulouse, 2005.

[50] Botto, L., *introduction to turbulence new notes*, Lecture Notes, 2016.

[51] Kolmogorov A. N., *The local structure of turbulence in incompressible viscous fluid for very large Reynolds numbers*, C.R. Acad. Sci. USSR 30. 301

[52] Veynante D., *Introduction to Turbulent Combustion*, VKI Turbulent Combustion Lecture Series, 2013

[53] Warnatz, J., Maas, U. and Dibble, R.W., *Combustion: Physical and Chemical Fundamentals, Modelling and Simulation, Experiments, Pollutant Formation*, Springer, Berlin, 2012.

[54] Jones, W.P. and Launder, B.E., *The Prediction of Laminarization with a Two-Equation Model of Turbulence*, International Journal of Heat and Mass Transfer, 15, 301-314, 1972.

[55] Shih, T.H., Liou, W.W., Shabbir, A., Yang, Z. and Zhu, J., *A New k-ε Eddy Viscosity Model for High Reynolds Number Turbulent Flows*, NASA TM 106721, 1994.

[56] Wilcox, D.C., *Turbulence Modelling for CFD*, DCW Industries Inc., California, 1998.

[57] Star CCM+ User Guide, 2016.

[58] Turns, S., A*n Introduction to Combustion: Concepts and Applications*, McGraw-Hill, Columbus, 2011.

[59] Spalding, D.B., *Mixing and Chemical Reaction in Steady Confined Turbulent Flames*, 13th Symposium on Combustion of the Combustion Institute, Pittsburgh, USA, 1970.

[60] Hautman, D.J., F.L. Dryer, K.P. Schug ve I. Glassman, *A Multiple-Step Overall Kinetic Mechanism for the Oxidation of Hydrocarbons*, Combustion Science and Technology, 25, 219-235, 1981.

[61] Libby P.A., and Williams F.A., *Turbulent Combustion: Fundamental Aspects and A Review*, Academic Press London, 1994

[62] Schmidt, D.P., Nouar, I., Senecal, P.K., Rutland, C.J., Martin, J.K., Reitz, R.D. and Hoffman, J.A., *Pressure-Swirl Atomization in the Near Field*, SAE Paper 990149, 1999.

[63] O'Rourke, P.J. and Amsden, A.A., *The TAB Method for Numerical Calculation of Spray Droplet Breakup*, SAE Paper 872089, 1987.

[64] Bai, C. and Gosman, A.D., *Development of Methodology for Spray Impingement Simulation*, SAE Paper 950283, 1995.

[65] Foucart, H., *Private Communications in CD-Adapco Department of Development*, 2016.

[66] Fluent User Guide, 2016.

[67] Schneider E., Maltsev A., Sadiki A., Janicka J., *Study on the Potential of BML-Approach and G-Equation Concept-Based Models for Predicting Swirling Partially Premixed Combustion Systems: URANS Computations*,

Combustion and Flame Vol.152, 2008

[68] Star CCM+, *Current Release Information on Reacting Flows*, 2016.

[69] (2007) Available at: https://community.dur.ac.uk/suzanne.fielding/teaching/BLT/sec1.pdf (Accessed: 24 August 2016).